CONTRACTOR REPORT

SAND91—7008
Unlimited Release
Patent Interest
UC—237

Facet Development for a Faceted Stretched-Membrane Dish by SAIC

Science Applications International Corporation
Energy Projects Division
10343 Roselle St., Suite G
San Diego, CA 92121

Prepared by Sandia National Laboratories Albuquerque, New Mexico 87185 and Livermore, California 94550 for the United States Department of Energy under Contract DE-AC04-76DP00789

Printed October 1991

PATENT INTEREST

A disclosure of invention relating to the subject of this publication has been filed with the US Department of Energy.

Issued by Sandia National Laboratories, operated for the United States Department of Energy by Sandia Corporation.

Printed in the United States of America. This report has been reproduced directly from the best available copy.

Available to DOE and DOE contractors from
Office of Scientific and Technical Information
PO Box 62
Oak Ridge, TN 37831

Prices available from (615) 576-8401, FTS 626-8401

Available to the public from
National Technical Information Service
US Department of Commerce
5285 Port Royal Rd
Springfield, VA 22161

NTIS price codes
Printed copy: A05
Microfiche copy: A01

Distribution
Category UC-237

SAND91-7008
Unlimited Release
Printed October 1991

FACET DEVELOPMENT FOR A FACETED STRETCHED-MEMBRANE DISH BY SAIC

Science Applications International Corporation
Energy Projects Division
10343 Roselle St., Suite G
San Diego, CA 92121

Sandia Contract: 42-8914A

ABSTRACT

The concept for a multi-facet stretched-membrane dish concentrator could reduce the cost and weight of solar thermal dish systems. A stretched-membrane mirror facet for such a multi-facet solar dish concentrator has been developed by Science Applications International Corporation (SAIC). Twelve of the 3.7-m diameter facets will be used to form a 115-m^2 dish concentrator, providing 75 kW_{th} to operate a 25-kW_e Stirling engine for electric power production.

The facet SAIC designed is focused using a vacuum system to elastically deform the thin (0.003-inch thick) stainless steel facet membranes. Elastic focusing was chosen over plastically deforming the membrane to a parabolic shape because it results in a simple manufacturing process. The SAIC facet can be focused from infinity to a minimum focal length-to-diameter ratio of about 2.7. Analytical design studies and experimental tests were performed to evaluate stresses in the ring and membranes during operation, the effects of strain cycling on the reflective surface, and to measure the optical quality of the mirror facets.

SAIC produced two prototype mirror facets and they were optically tested at the Solar Energy Research Institute and at Sandia National Laboratories. The first facet showed slope errors ranging from 2.95 to 3.3 mrad over the f/d range of 2.7 to 3.0.

Acknowledgments

This work was supported by the U.S. Department of Energy through Sandia National Laboratories under contract 42-8914A. The authors thank Dr. Thomas R. Mancini and the Solar Thermal Technology staff at Sandia National Laboratories.

CONTENTS

LIST OF FIGURES

LIST OF TABLES

1.0 INTRODUCTION

Parabolic dish solar concentrators are used to reflect and concentrate solar energy on a receiver where the thermal energy is absorbed in a working fluid. The energy is subsequently converted to electricity by means of various conversion processes. Stretched-membrane dish solar concentrators offer a promising alternative to current glass/metal dish concepts in that they are potentially lighter in weight and less costly. However, technical and developmental questions exist regarding the best approach for the membrane reflector configuration. Although a single-facet design can achieve higher solar concentration and possibly lower costs than a multi-facet design, multi-facet concentrators benefit from easier fabrication, convenient field assembly and use of more near-term technology.

The purpose of the "Stretched-Membrane Facet Development Project" is to design and fabricate a high quality, low cost, and low risk multi-faceted stretched-membrane dish for near-term applications. The concentrator has been designed for integration with an advanced solar receiver and a Stirling engine/generator in a 25 kW_e modular power production unit. The conceptual design of the twelve-facet, 115-m^2 concentrator is shown in **Figure 1.0-1**. The twelve facets provide approximately 75 kW_{th} to the Stirling engine.

The dish development project is comprised of two phases with the end goal of producing a fully-integrated faceted concentrator for testing at Sandia's Solar Thermal Test Facility (STTF). This report documents work accomplished by Science Applications International Corporation (SAIC) in the first phase of the project. During Phase I, SAIC and Solar Kinetics Incorporated (SKI) developed and fabricated 3.7-m diameter stretched-membrane mirror facets for optical evaluation at SERI and Sandia. Concurrent with the facet development, W G Associates designed a facet support structure and concentrator drive pedestal. The facet support structure and drive pedestal were designed to meet specific criteria, such as providing ground level accessibility to the receiver/engine, inverted or vertical concentrator stow, and low cost. The current state-of-the-art dish solar concentrator is the glass/metal McDonnell-Douglas dish. The McDonnell-Douglas dish concentrator support structure/pedestal was the basis for comparison with the proposed support structure concepts. In Phase 2 of the project, one or more faceted stretched-membrane dishes will be fabricated and installed at the DOE National Solar Thermal Test Facility at Sandia National Laboratories in Albuquerque, NM. After initial testing of the dish, Sandia will integrate the faceted concentrator with a receiver and a Stirling engine for additional system testing.

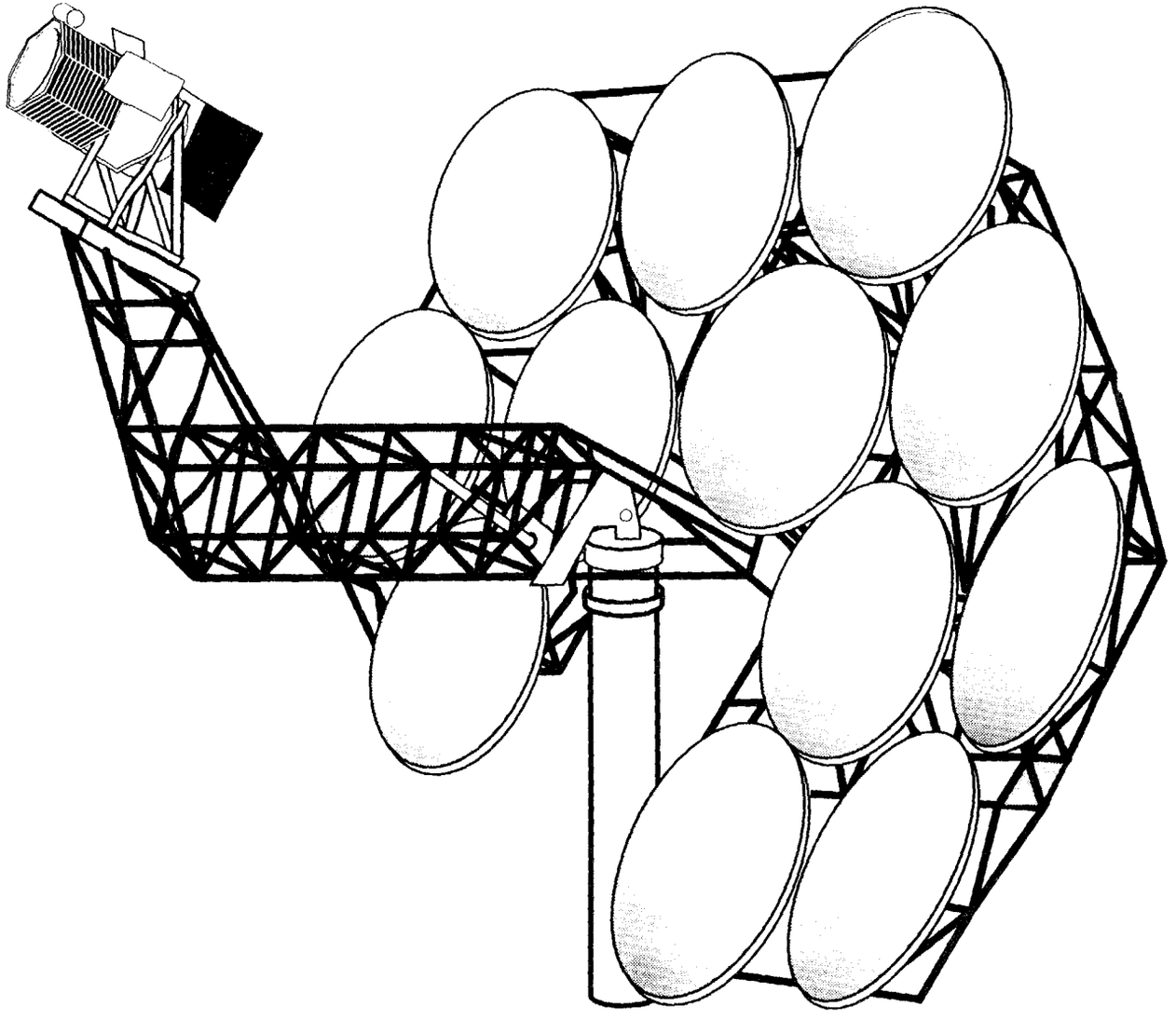

Figure 1.0-1. Conceptual Design of the 115-m^2 Stretched-Membrane Dish Concentrator

2.0 STRETCHED-MEMBRANE FACET DESIGN DESCRIPTION

A stretched-membrane facet comprises two thin metal membranes stretched over each side of a large diameter metal ring. The reflective surface is a silvered polymer film laminated onto the front membrane. One of the facets fabricated in this project is shown in **Figure 2.0-1.** A vacuum in the space between the two membranes draws the reflective surface down to form a concave focused shape. Although not implemented in the current control system design, the space between the metal membranes can also be quickly pressurized to defocus the mirror for safety procedures. The solar concentrator comprises twelve facets, each 3.7-m in diameter. The twelve facets are arranged in a modified hexagonal-close-pack array in a compromise between a parabolic and a spherical contour. The facet array is mounted on a support structure as depicted in **Figure 1.0-1.** The 3.7-m diameter facet size is the maximum size that can be readily transported from the factory to the concentrator assembly site. Twelve facets are required to provide a peak power of about 75 kW_{th} to the receiver. A central vacuum system is used to draw the appropriate vacuum level in each module to produce the required focal-length-to-diameter ratio (f/D), which varies from 2.7 to about 3.1, depending on the position of the individual facet in the array of twelve. In the following subsections, the mirror module, focus control system, and support structure interface are described.

2.1 Mirror Module Design

The design of the concentrator facet is an extension of previous stretched-membrane mirror module designs developed under Sandia/DOE sponsored heliostat programs.[1,2] An eight-inch deep I-beam was selected for the ring for the facet fabricated on this program. The eight-inch depth of the ring was selected based on avoidance of front and back membrane contact during focussing (at the minimum focal length required for this dish design the front membrane center deflection is 8.26-cm (3.25-in). Because of this, the ring stiffness and strength is higher than required based on deflection and stress criteria. No extra material is required to provide adequate stiffness to accommodate the asymmetrical facet support points. The ring for the prototype facet is an M8X6.5 "Junior I-Beam" with dimensions of 20.3-cm x 5.8-cm (8.0-in x 2.28-in) with a web thickness of 3.43-mm (0.125-in). The I-beams are manufactured from A36 carbon steel, and weigh 6.5 pounds per foot. To fabricate the ring, three sections were rolled to an outside radius of 1.858-m (73.13-in) with an inside radius of 1.80-m (70.85-in) and welded together.

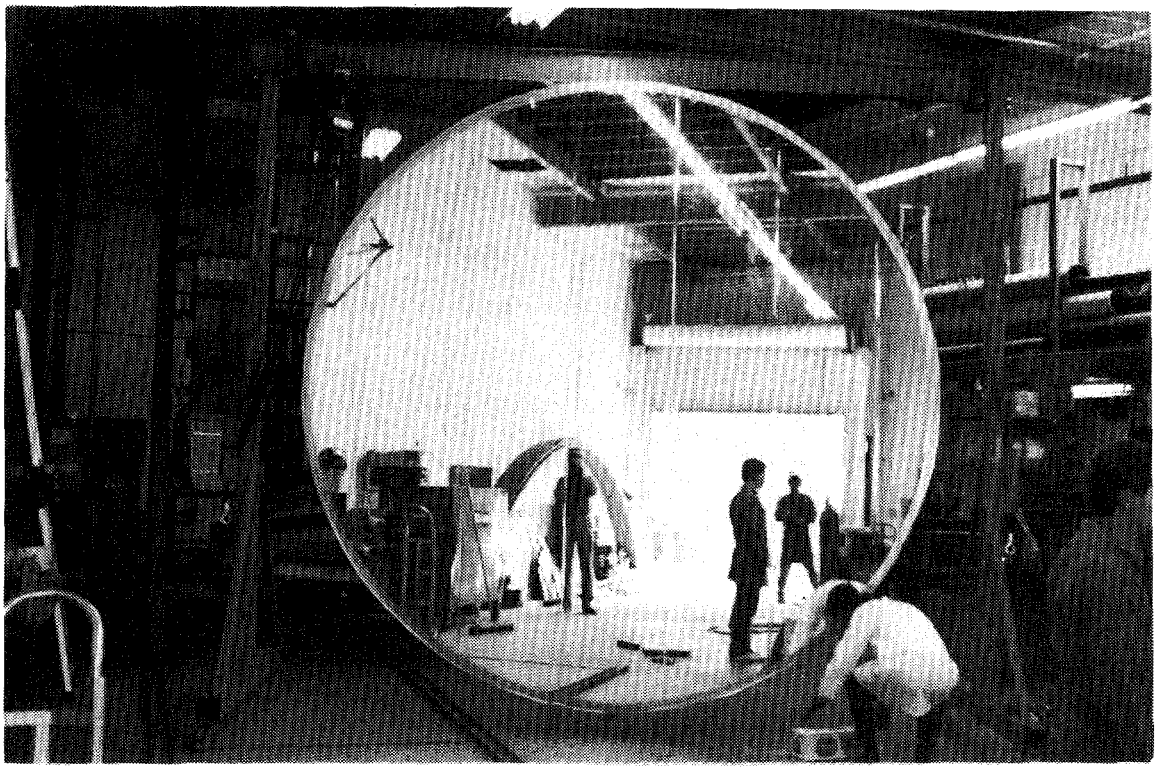

Figure 2.0-1. Facet for Faceted Stretched-Membrane Dish

The membranes used for the facets are 0.076-mm (0.003-in) thick Type 201 stainless steel in the half-hard condition. The minimum yield strength of this material is 827 MPa (120,000 psi). The membranes are pretensioned to a level of 138 MPa (20,000 psi), and reach a maximum stress of 620 MPa (90,000 psi) under worst case focus and wind load conditions. The membranes are fabricated from flattened stainless steel coil stock that is 61-cm (24-in) wide. The strips of stainless steel are welded together with a roll-resistance seam welder. The front membrane is laminated with reflective film prior to welding. The membranes are laminated with ECP 305 Silverized Polymer Reflective Film, manufactured by the 3M Company. The rolls of reflective film are cut to a 55.2-cm (21.75-in) width and laminated to the front stainless steel membrane in the space between the roll resistance seam welds. ECP 244 Aluminized Polymer Film was used as a tape to bridge adjacent reflective film strips over the seam weld. The tape was also used around the perimeter of the facet to seal the outer edges of the reflective film. The front and back steel membranes are welded to the facet ring using a hand-held roll-resistance welding system developed by SAIC. A weight breakdown for the facet is shown in **Table 2.1-1**. It should be noted that the minimum ring weight is constrained by the commercially available sections at the required height, not by strength considerations.

Table 2.1-1 Facet Weight Breakdown

Ring	107.5 kg (237.1 lb)
Membranes	12.5 kg (27.6 lb)
Brackets	7.0 kg (15.4 lb)
Hardware	3.2 kg (7.1 lb)
Focus Control	2.0 kg (4.4 lb)
TOTAL	132.2 kg (291.6 lb)

2.2 Focus Control System Design

The facets are focused to the proper curvature by pulling a vacuum between the front and back membranes of the facet. A central blower is used with hoses extending to each facet to induce the vacuum. The device used to maintain the proper curvature of the facet is shown in **Figure 2.2-1**. A tubular steel arm extends from the facet ring to the interior of the facet and supports a focussing valve. The tube acts both as structural support for the valve and as an air duct. The valve is an SAIC proprietary design that provides reliable and repeatable focussing of the module. Contact with the front membrane modulates the airflow and maintains the proper membrane position. The focus

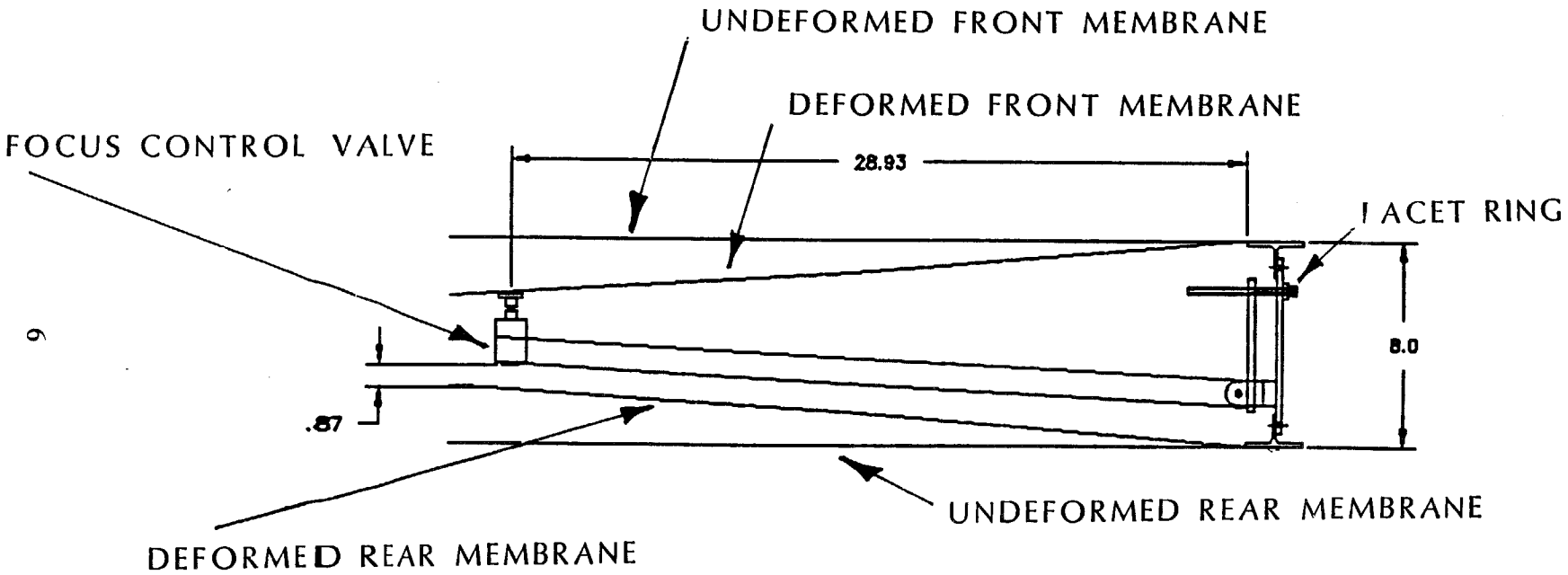

Figure 2.2-1. Facet Focus Control Assembly

assembly shown is adjustable to allow changes in the focal length of the mirror. The focussing system described has been tested and has shown to be reliable and low cost.

A single stage blower is used to provide the vacuum to the facets. The blower has a peak power consumption of 200 watts. One inch diameter flex hoses are routed to each of the twelve facets from the central blower. The blower maintains a vacuum of approximately 4140 Pa (.6 psi) to the plenum. During testing the facet was found to be virtually vacuum tight, therefore introduction of a controlled leak was necessary in order to allow the facet to adapt to dynamic conditions, such as changes in wind speed and direction. The system has the capability to reverse flow, pressurizing the plenum to produce a convex shape that will disperse the beam away from the receiver. However, this capability was not implemented in the Phase 1 facet design.

2.3 Support Structure Interface Design

The facets each have three radially and circumferentially adjustable mounting points located on the facet ring. The adjustment capability is required in order to allow alignment of the facet support points with the support structure, and alignment of the reflected beam on the receiver. The hardware located at each attachment point is shown in **Figure 2.3-1** and **Figure 2.3-2**. Brackets are welded to the web of the facet ring at three points, as shown. A 3/4-inch rod end is attached to the bracket with a 3/4-inch shoulder bolt. The female rod end is attached to a 3/4-16 steel shaft and two hex nuts that provide attachment to the support structure. The support structure has oversized holes to allow for adjustment of the mounting location. The rod end allows the shaft to rotate freely in all directions for proper placement and alignment of the facet.

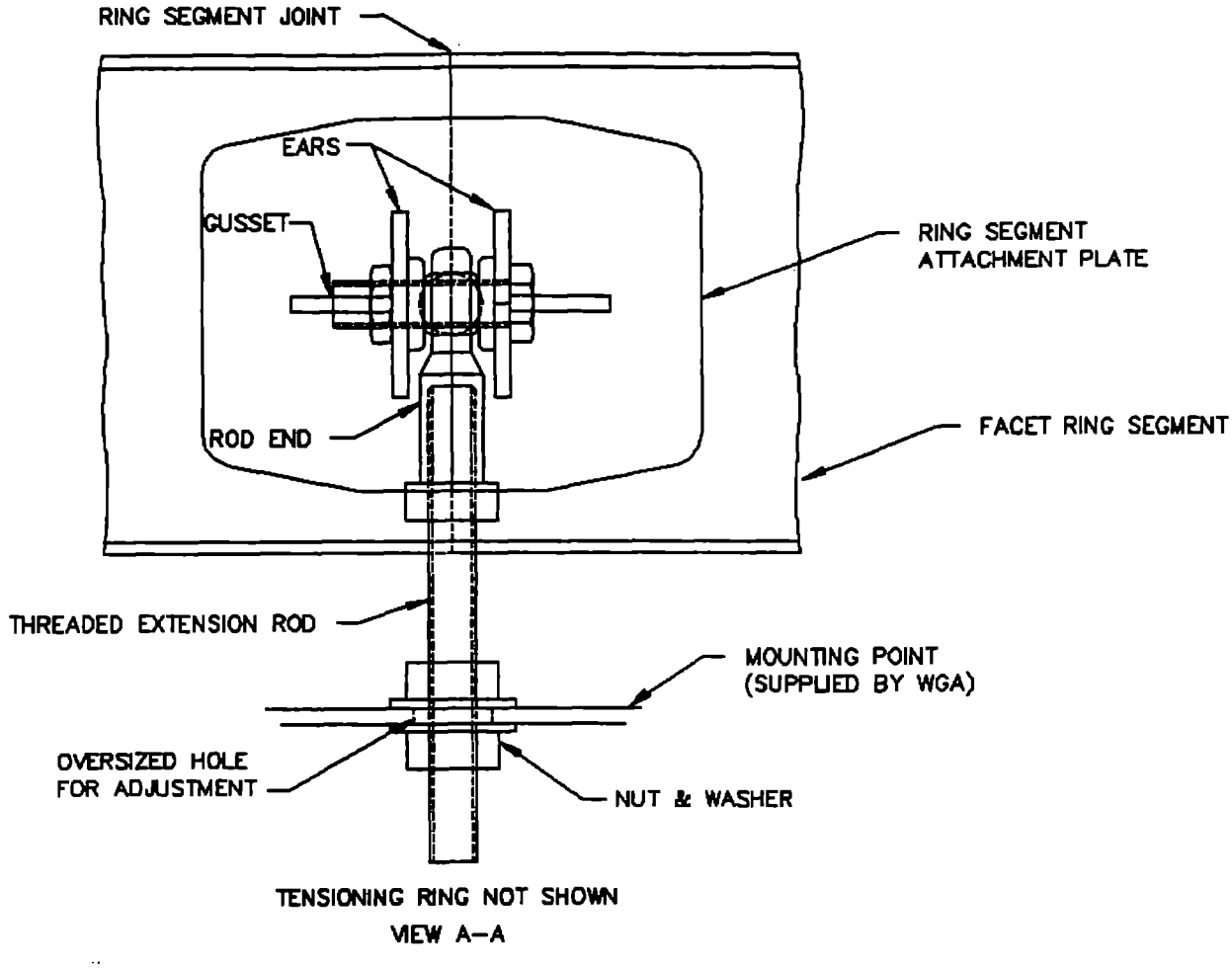

Figure 2.3-1. Ring-Support Structure Interface Assembly - Front View

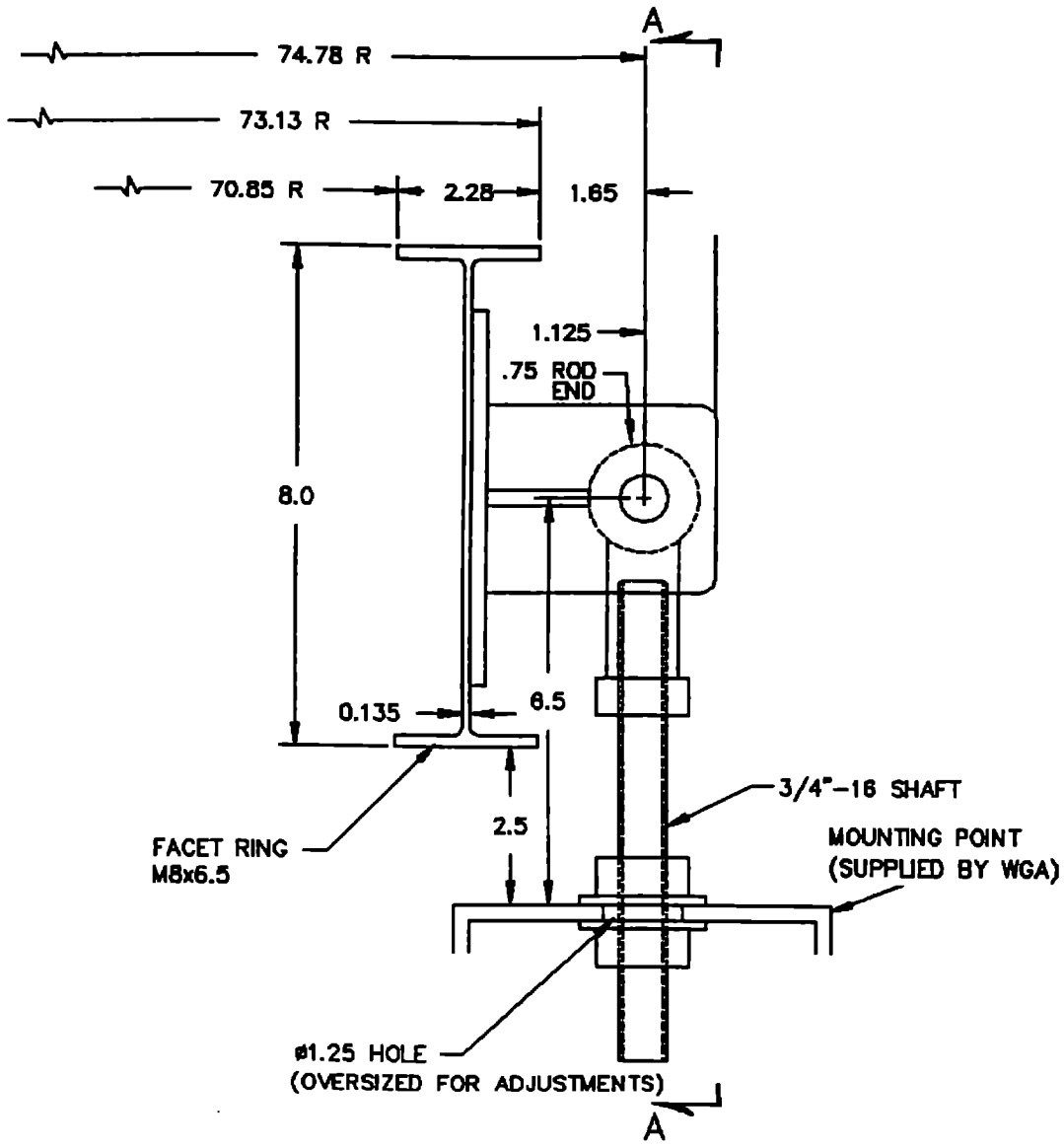

Figure 2.3-2. Ring-Support Structure Interface Assembly - Side View

3.0 FACET DESIGN SELECTION AND ANALYSIS

3.1 Facet Concept Selection

Stretched-membrane mirror facets can be formed either by plastically pre-forming the membrane into a parabolic shape or by a method in which a pressure-induced elastic deformation of an initially flat membrane occurs, which results in a near spherical shape. In the plastic deformation approach, a metal membrane with a relatively low yield strength is used to form the facet surface by applying a pressure differential across the membrane in order to permanently deform the membrane into the proper shape. Once the pressure differential is released, the membrane does not return to its initially flat configuration. In the elastic deformation approach, a pressure differential is applied across an initially flat membrane to temporarily deform the membrane to the proper shape during operation. In this case, the deformation stress in the membrane does not reach the yield strength of the membrane material, and the membrane returns to its original, flat configuration once the pressure differential is removed.

At focal-length-to-diameter (f/D) ratios greater than 1.0, the performance difference between the shapes resulting from the elastic and plastic deformation fabrication methods may be small. In a multi-facet dish design, a single facet dish with a small f/D is emulated using multiple small diameter, shallow (i.e., large f/D) facets. For example, in the present twelve-facet dish, the individual facet f/D range is from 2.7 to 3.1. Thus, because the f/D ratios of the individual facets are relatively large, elastic deformation of an initially flat membrane can be used to form the facets of a multi-facet dish.

The elastic deformation approach was selected by SAIC for the facets of the multi-facet dish. A major reason for this choice is the elimination of the additional manufacturing step required to plastically deform the facets to the proper focal length. Also, once a membrane has been plastically deformed, it is fragile and more susceptible to wrinkles and the effects of winds. With SAIC's elastic membrane deformation approach, the facets may be relatively easily manufactured at a central site and shipped to the installation site with normal shipping procedures. Once the facets are installed on the support structure, the pressure differential is applied through the central vacuum system to achieve the proper focal length of each facet.

SKI chose to pursue the plastic deformation approach. As predicted at the beginning of the project, both facet designs met the optical accuracy requirements of the project, but SKI's facets had a slightly

higher accuracy. The higher accuracy is due to the more exact parabolic shape that can be achieved through plastic deformation. However, the SKI design requires additional components to protect the plastically deformed membranes from damage during non-operating periods in addition to the extra manufacturing steps required to plastically deform the membranes.

3.2 Ring Selection

The materials available for fabrication of the ring for the mirror facet are:

1. A500 carbon steel,
2. A500-B carbon steel,
3. A36 carbon steel, and
4. stainless steel.

The A36 carbon steel is the lowest cost option, with the A500 and A500-B carbon steel having progressively higher yield strength with an increase in cost. Although stainless steel would be the ideal ring material from a fabrication point of view, due to compatibility with the membranes for welding and matching thermal expansion coefficient between the ring and membranes, the cost of stainless steel is prohibitive for this application.

Because the selection of the ring size was driven by the physical requirements for focussing and not by strength considerations, the ring material strength is not a significant issue. Based on cost considerations, A36 carbon steel was selected for fabrication of the ring. This material selection results in a minimum ring cost, but requires welding of dissimilar metals and consideration of the effects of a difference between the thermal expansion coefficients of the membrane and ring. Studies carried out as part of the "Improved Design for Stretched-Membrane Heliostats" program [2] successfully resolved the problems associated with welding of different metals. The thermal expansion coefficient mismatch between the ring and the membrane leads to varying stress levels in the membranes. These were determined to be within reasonable bounds and could be compensated for by the facet focus control systems. [2]

Considerations for selecting the type of cross section for the ring include:

1. maximization of the facet out-of-plane stiffness per unit weight;
2. the ring must provide a surface for in-plane rigid attachment of the membranes;

3. the use of conventional beam forming and ring rolling techniques to achieve the required tolerance;
4. the ring must provide adequate in-plane buckling and torsional stability; and
5. the ring must provide adequate spacing between the membranes for focussing.

The ring cross sections available are square tube, rectangular tube, I-beam, channel, round tube and nested channels. A channel cross-section and I-beam were considered the two best candidates for the ring design. In order to limit the ring weight while achieving the eight inch membrane spacing required for focussing, an I-beam cross-section was used in our initial concept rather than a rectangular tube. An I-beam has considerably less torsional stiffness than a tube. However, in the stretched-membrane configuration, the membranes supply nearly all the torsion stability for the facet ring.

The structural properties of the I-beam selected for the facet ring are shown in **Table 3.2-1**. The selected I-beam was the widest commercially available structural shape that met the eight-inch depth criteria. Additional weight savings would be available if a custom I-beam or channel with a thinner wall were fabricated for the ring.

Table 3.2-1 Facet Ring Structural Properties

Beam Designation	Depth	Width	Web Thickness	Flange Thickness	Fillet Distance
M8X6.5	8.00 in	2.281 in	.135 in	.189 in	.500 in

Cross-Sectional Area	$A = 1.920\ in^2$		
Torsional Constant	$J_1 = .020\ in^4$		
Moment of Inertia	$I_x = 18.500\ in^4$	$I_y = .343\ in^4$	
Section Modulus	$S_x = 4.620\ in^3$	$S_y = .301\ in^3$	

Poisson's Ratio = .300

3.3 Membrane Selection

After extensive evaluation, stainless steel foils were selected over other membrane materials in earlier SAIC stretched-membrane heliostat efforts. Stainless steel foils with the proper mechanical properties are available for facets that incorporate the elastic deformation approach. Since such good results have been achieved with stainless steel in SAIC's heliostat efforts [1] and because the requirements for stretched-membrane dish facets are similar for stretched-membrane heliostats, stainless steel was selected as the membrane material for this effort.

The factors considered in selecting the type stainless steel, hardness and thickness, were

1. adequate yield strength to survive the required elastic deformation for focussing and the wind loading in any orientation;
2. ability to weld the membrane material;
3. ability to handle the membrane material;
4. flatness of manufactured coil stock;
5. adequate margin between yield strength and ultimate strength;
6. cost; and
7. optical quality considerations.

At the minimum required facet f/D of 2.7, the resulting membrane stress due to elastic deformation is 607 MPa (88,000 psi). This assumes an initial pretension of 138 MPa (20,000 psi) prior to out-of-plane deformation. Half-hard stainless steel foil with a yield strength of 827 MPa (120,000 psi) is adequate to withstand the front membrane stress for an f/D of 2.7 with a safety factor to yield of 1.4. The analysis methodology and results are discussed further in Section 3.4-1.

To limit the vacuum required for focussing the facet, limit the ring compression, and obtain the best optical quality, the thinnest practical membrane was desirable for the facet. SAIC has previously successfully fabricated membranes from half-hard stainless steel foils 3-mils thick. The welding of foils less than 3-mils thick is difficult and quality control is difficult to maintain. Therefore, 3-mils thick, half-hard stainless steel was selected for the facets.

SAIC has previously performed weld and corrosion tests on Type 201 stainless steel foil to determine its usefulness in heliostat application. This type of stainless steel has a lower chromium content and about a 25% lower cost than the Type 304 stainless steel used previously for heliostat membranes. Type 201, 304 and the low carbon version 304L stainless steels were considered for use on the facet for this project. Type 201 was selected as the preferred material.

The stainless steel membrane material has a coefficient of thermal expansion of 16.6×10^{-6} cm/cm-°C (9.2×10^{-6} in/in-°F), as compared with the carbon steel ring material with a coefficient of 14.8×10^{-6} cm/cm°C (8.2×10^{-6} in/in-°F). The higher coefficient of thermal expansion for the stainless steel results in an increase in membrane tension as the operating ambient temperature drops from that at which the facet was the manufactured and in a reduction in membrane tension as the ambient temperature increases above the manufacturing temperature. A finite-element model was used in the "Improved Design for Stretched-Membrane Heliostats" program to determine the changing tension effects due to the dissimilar thermal expansion coefficients.[2] The variation of the membrane tension as a function of temperature is shown in **Figure 3.3-1**. The variation in ring and membrane stresses as a function of ambient temperature is sufficiently small so that the variation in thermal expansion coefficients is not a problem.

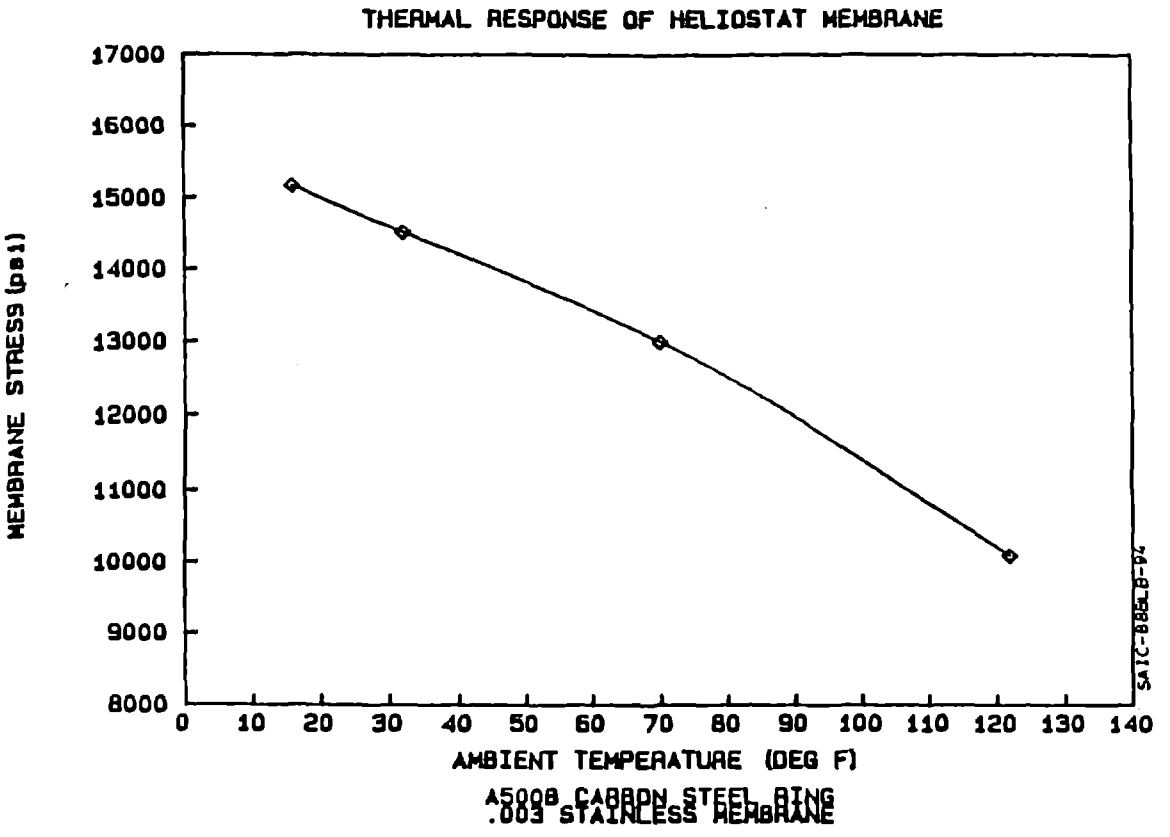

Figure 3.3-1. Thermal Response of Stainless Steel Membrane Welded on a Carbon Steel Ring

3.4 Structural Analysis

Although SAIC has gained significant experience designing and fabricating mirror modules from its Stretched-Membrane Heliostat programs, the mirror modules (facets) for the "Stretched-Membrane Facet Development Dish Program" presented some unique structural challenges. The minimum facet f/D ratio of 2.7 requires a center membrane displacement of 8.3-cm (3.25-in). This displacement produces strain levels in the facet membranes that are significantly higher than those encountered in heliostat mirror modules. These high strain levels produce high stress levels in the membranes. Structural analysis was performed on the facet ring and membranes in order to quantify and evaluate the effects of this high strain. Analysis was also performed on the attachment brackets to evaluate operational and survival stresses and deflections.

3.4-1 Membrane Analysis

The environmental requirements state that the mirror module must maintain focus under an average of 13-m/s (29 mph) wind, and maintain structural integrity in a non-operational state in any orientation in a 22-m/s (47 mph) wind. Survival in the horizontal stow position in a 40-m/s (90 mph) wind is required. The worst loading from a structural and operational standpoint occurs when the wind is perpendicular to the membrane surface with the front membrane downwind.

Wind load analyses performed during SAIC's Stretched Membrane Heliostat projects have shown that the wind plays a significant role in the design of the mirror modules and related structural components.[1,2,5] Due to the smaller size and higher membrane-stress levels in the facets for the faceted stretched membrane dish, the wind plays a much smaller role in their design. Analysis showed that under worst case operational wind loads of 13-m/s (29 mph), the stress caused by the wind was on the order of 10% of the operational membrane stresses. Therefore, while the added membrane

stresses caused by wind load was included in the design calculations, it did not play a significant role in the facet design.

The ideal shape for the reflective surface of an on-axis facet is a perfect parabola. The closer the focused membrane shape approaches a perfect parabola, the more accurate the facet. The goal of this project was to achieve the most accurate focused membrane shape while remaining within the physical constraints of the chosen materials. Analytical work performed by L.M. Murphy, [3] shows that the shape of a membrane deformed under uniform pressure more closely approaches a perfect parabola as the membrane pretension increases. Therefore, the facet was designed with the highest possible pretension in order to produce maximum surface accuracy without yielding the membrane.

Based on the assumption of a spherical membrane shape, the maximum membrane center displacement for a f/D ratio of 2.7 was found to be about 8.3-cm (3.25-in). The following relation was used to obtain the maximum membrane stress:[4]

$$S = 0.965 \frac{Et^2}{a^2} \frac{Y^2}{t} \qquad (1)$$

where S = maximum membrane stress (psi),
E = modulus of elasticity (psi),
t = membrane thickness (in),
a = membrane radius (in), and
y = membrane center displacement (in).

Equation (1) is based solely on the material properties and maximum center displacement of the membrane. There is no consideration in this relation for the membrane pretension T_0. To approximate the actual maximum membrane stress, the in-plane stress created by the pretension was added to the stress caused by the membrane deformation. It was determined that, with a pretension of 138 MPa (20,000 psi), the maximum membrane stress was approximately 550 MPa (80,000 psi).

Adding an additional 10% for operational wind loads increased the maximum membrane stress to 605 MPa (88,000 psi).

During facet focussing, the front and rear membranes are subject to a uniform internal pressure (neglecting wind effects). This pressure produces elastic axisymmetric deformations of both membranes. To size the blower motor and evaluate the membrane response to this uniform pressure, the following pressure-displacement relation was used.[3] This relation is based upon an extension of a simple design relation developed using a variational approach.

where $P = (4T_0/a)(y/a) + 3.44(Et/a)(y/a)^3$ (2)

P = applied uniform pressure (psi),

T_0= initial membrane pretension (force/length) (lb/in),

Y = membrane center displacement (in), and

A = membrane radius (in).

By inspection of equation (2), it can be seen that there are two distinct components. The first term is based solely on pretension and membrane geometry. The pretension provides a geometric stiffness effect to the overall membrane stiffness. The second term in the equation is based on material properties and geometry and represents the material stiffness effect. For the current facet configuration, this relationship predicts a required pressure of 4140 Pa (0.6 psi) for the smallest facet f/D of 2.7.

In the formulation of equations (1) and (2) for membrane displacement, an assumed membrane shape was used. In the Roark and Young formulation, [4] the membrane shape was assumed to be as follows:

where $y = \max y\ (1 - (0.9r^2/a^2) - (0.1r^5/a^5))$ (3)

r = distance from center (in),

y = membrane displacement at distance r from center (in),

max y = membrane center displacement (in), and

a = membrane radius (in).

In Murphy, [3] the membrane shape was assumed to behave as

$$y = \max y \, (1 - (r^2/a^2)) \qquad (4)$$

where all variables are defined above in equation (3).

Neither of these shape relations take into account the geometric stiffness effect due to pretension. The membrane shape remains the same regardless of the pretension. In order to more accurately quantify the geometric stiffness effect as it relates to the deformed membrane shape, it would be necessary to develop a non-linear, large deflection finite-element model. This analysis technique was not developed for this phase of the project due to time and budget constraints.

3.4-2 Ring Analysis

The depth of the facet ring was determined by the requirement for the front and rear membranes to deform during focussing and not come in contact with each other. This led to the use of a 20.3-cm (8-in) deep ring segment. Analysis of various ring segments showed that a 20.3-cm (8-in) depth was not necessary to assure proper strength and stiffness. To validate the selection of an 8-in ring segment, analyses were performed on the ring section to assure adequate stiffness, strength, and stability. A two-dimensional axisymmetric finite-element model was performed to evaluate the ring roll and stresses. A buckling analysis was performed to evaluate stability. The finite-element model was made of two-dimensional axisymmetric elements. The material was carbon steel. The I-beam section was held at the center of the web to simulate the attachment points. The membrane load was applied at the upper and lower corner elements of the beam flange at an angle of attack of 5.3 degrees. The magnitude of the applied force was determined to be 50,000 N/radian (11,180 lb/radian).

The results of this analysis showed that the ring is able to withstand the membrane loading without significant stress or deflections. The maximum von Mises stress in the ring segment was determined to be 159 MPa (23,000 psi). The maximum deflection in the ring was determined to be 1.4-mm (0.056-in).

Further investigation of the analysis results showed that the majority of the stress in the ring was caused by the circumferential compression in the flanges. As the membranes are stressed, they compress the ring. **Figure 3.4-2** shows the facet ring finite element model with displacement magnitude shading. The displacements shown in this figure are scaled 20X.

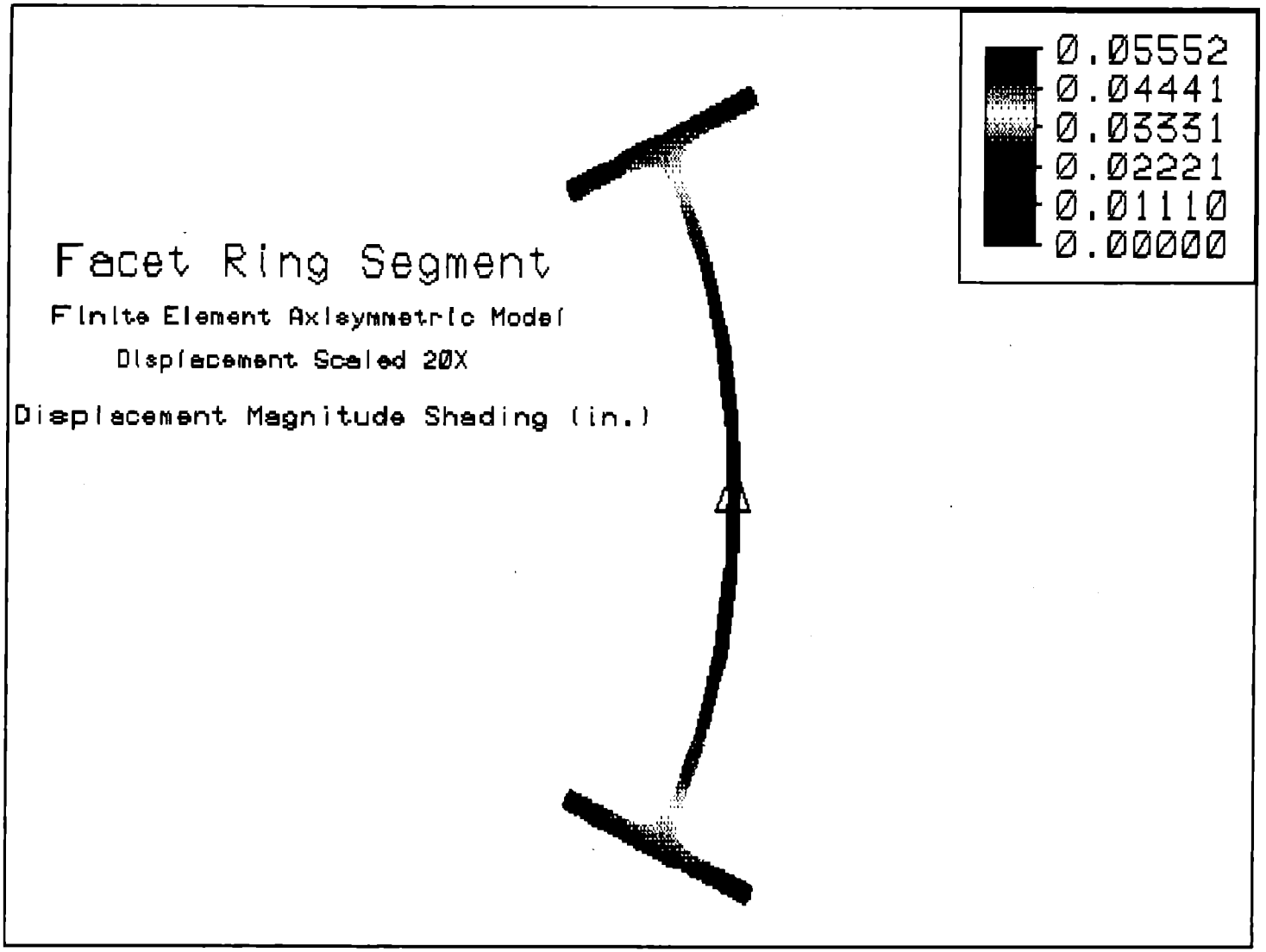

Figure 3.4-1. Results of Finite Element Modeling of Facet Ring

3.4-3 Attachment Bracket Analysis

Analysis was performed on the attachment brackets to evaluate stresses and deformations under various loading conditions. The maximum deflections in the attachment brackets under gravity and wind loading were found to be 1.1-mm (0.043-in). The stresses associated with these very small deflections were found not to be significant based on the strength of the materials used.

3.5 Facet Focus Control System Selection

A differential pressure must be maintained across the front membrane of the facets in order to achieve the proper focal lengths. For a 3.7-m diameter facet with an f/D of 2.7, a pressure differential of about 4140 Pa (0.6 psi) is required for facets made with .003 in thick stainless steel membranes. This pressure differential is an order of magnitude higher than that required for heliostat applications. Therefore, external membrane pressure changes due to wind loading have substantially smaller effects on facet focal length than the wind effect on heliostats.

The speed that the focus control system must react to external pressure changes has a direct effect on its design. The FOCUS computer program, originally written for the "Improved Heliostat Mirror Module Development Program", was used to quantify the effect of wind on facet focal length. The results of this analysis are shown in **Figure 3.5-1**. An option in the program was used in which the facet focal length can be set initially for no wind, and then allowed to vary as wind speed increases. As shown in **Figure 3.5-1**, with wind speeds in the operational range from 0 - 17 mph, wind has little effect on facet focal length. Again, this is because of the high initial pressure differential required to maintain the relatively short focal length of these mirrors.

Three basic configurations were considered for maintaining the vacuum in the facet plenum. These were 1) the use of a central vacuum pump or blower with vacuum hoses running to each mirror facet, 2) the use of a pump/blower on each individual facet for maintaining the vacuum, and 3) the use of a sealed plenum with a linear actuator to modulate the rear membrane and induce a pressure change in the facet interior (such as used by SAIC in our stretched-membrane heliostat design). The centralized vacuum pump/blower was selected because of its inherent lower cost, and the lack of need for movement of large volumes of air quickly during normal operation.

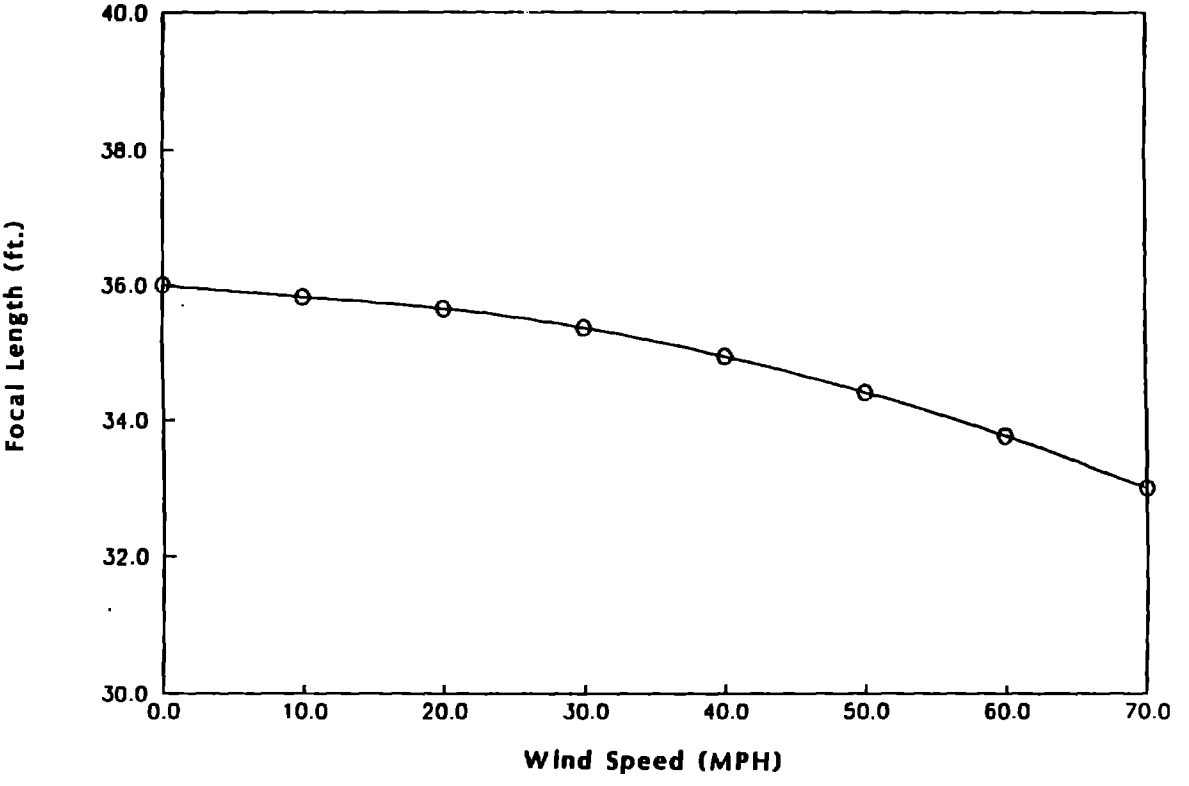

Figure 3.5-1. Non-Controlled Mirror Module Focal Length Variation with Wind Speed

Two configurations were considered for front membrane position sensors for vacuum control. These were 1) the use of an LVDT position indicator to provide a feedback signal to the central blower for control of the system pressure and 2) a passive design consisting of a mechanical valve located within each facet for plenum pressure control. The passive design was selected for implementation on this project.

The electronic feedback option for the focus control system is shown in **Figure 3.5-2.** It was assumed that three different facet focal lengths are required, indicated in the figure as focal zones 1, 2 and 3. In each focal zone, a LVDT membrane position indicator is shown on one facet only, termed the "master facet", to provide a feedback signal that determines the pressure in all four of the modules in that focal zone. This focus control system design was rejected because of the high costs of the electronic components, and the difficulties associated with balancing the facet pressures within each focal control zone.

A vacuum pump with 1/4-in diameter hose was used on the first test facet for maintaining the facet vacuum. It was determined that the flow rate available from the vacuum pump was inadequate for this application, and the vacuum capability was much higher than required. About one-half hour was required to pump the facet down to the required focal length from an initially flat configuration with the vacuum pump. During design of the second-generation facet, a higher volume blower was utilized with 1-in diameter flex hose. The vacuum capability of the blower was well suited to the requirements of focussing the facet. Approximately three minutes were required to evacuate the facet to the proper focal length with the blower configuration.

The final facet focus control system design consists of a central blower with 1-in diameter flex hose connected to each facet. A passive front membrane position sensing technique was chosen utilizing a mechanical valve located within each facet.

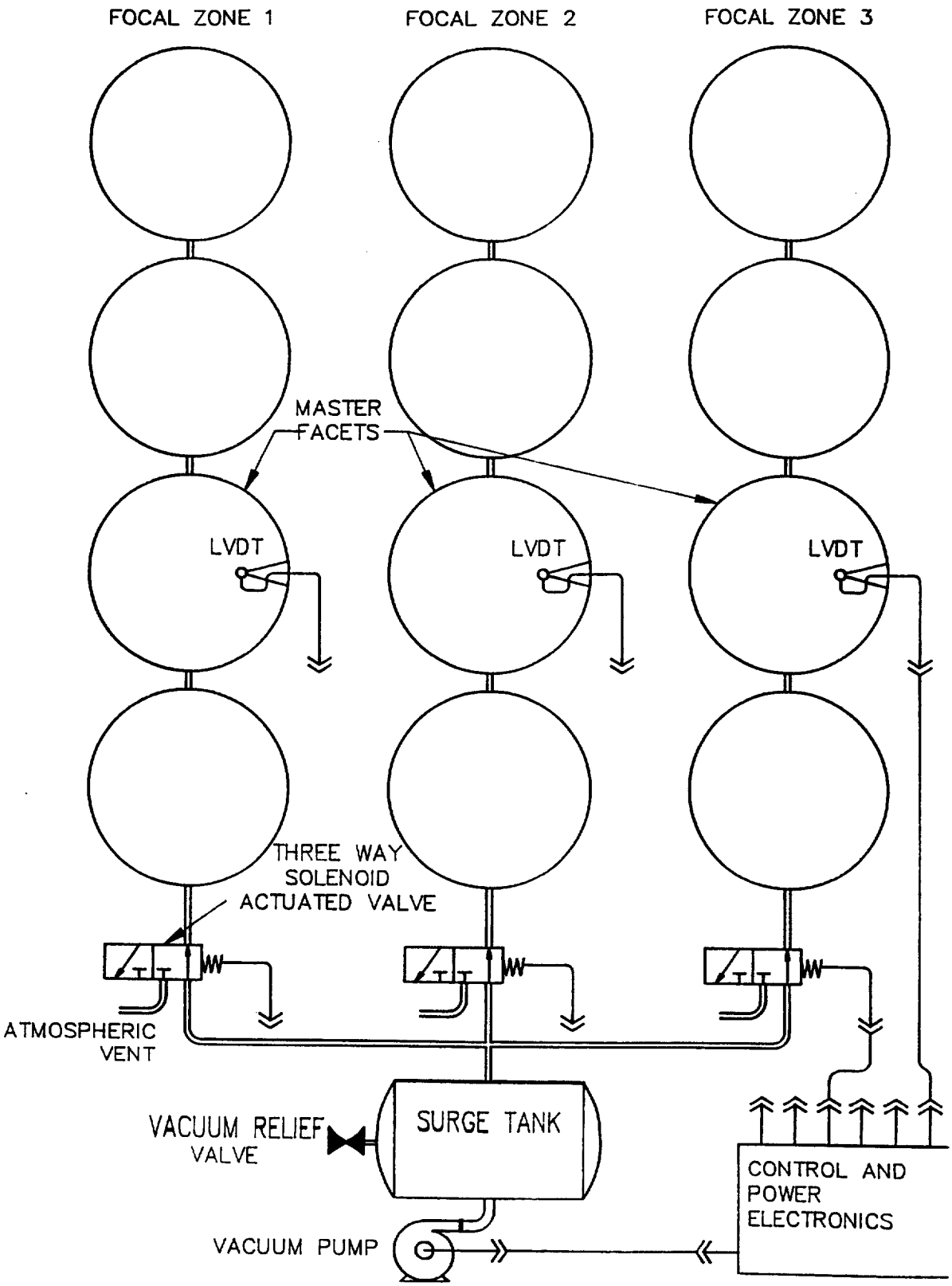

Figure 3.5-2. Electronic Feedback Focus Control System Diagram

4.0 LABORATORY TESTING AT SAIC

In Phase 1 of the "Stretched-Membrane Facet Development Project", SAIC performed tests to evaluate issues perceived as critical to the development of the SAIC design. The three main areas of testing were weld strength, laser ray trace optical evaluation, and membrane strain cycling. In the following sections, each of these testing efforts is discussed.

4.1 Weld Strength Testing

The elastic membrane deformation design approach for the facets requires the use of high yield-strength membrane material due to high operating stresses. The strength of the membrane-to-membrane welds and the membrane-to-ring welds were of concern under these high stress conditions. Therefore, SAIC performed weld strength tests to identify weld parameters and to verify that the weld strengths are adequate for this application.

The goal of the weld tests was to obtain quantitative data on weld parameters for the roll-resistance welding equipment and verify that the weld strengths will be adequate for the design stresses. Tests were performed on membrane-to-membrane and membrane-to-ring welds. SAIC uses a stationary roll-resistance welder for the membrane-to-membrane welds and a hand-held roll resistance welder for the membrane-to-ring welds. Both of these welders have been modified for these specialized applications. A systematic approach was used in isolating the effects of the various weld parameters on weld strengths. The weld parameters that were varied for the hand-held seam welder are shown in **Table 4.1-1**.

Table 4.1-1. Hand-Held Roll-Resistance Weld Parameters

Weld Type	Percent Current
Weld Time	Voltage
Pressure	Weld Speed
Head Thickness	Surface Preparation
Quenching	Inter-Layer
Tension Level	Ground Distance
Membrane Thickness	Ring Thickness

The weld parameters used for the stationary welder on the membrane-to-membrane welds are shown in **Table 4.1-2.**

Table 4.1-2. Stationary Roll-Resistance Welder Parameters

Squeeze Time	Percent Heat
Cool Heat	Wheel Speed
Heat Time	Pressure
Hold Time	Quenching
Off Time	Material Thickness
Impulses	

The weld samples were strength tested on a tensioning test fixture consisting of a hydraulic actuator, control valve, and a membrane gripping mechanism. The test fixture is shown in **Figure 4.1-1**. Beam sections identical to the facet ring were used for the membrane-to-ring welds. Two six-inch-wide strips of 3-mil 304, half-hard stainless steel were welded to the top and bottom flanges of the M8X6.5 I-beam section after the surfaces were ground and finished with 120 grit paper. The stress at weld failure during tests is calculated from the force of the hydraulic actuator and the weld sample width.

To limit the parameter ranges, preliminary tests were performed to obtain a "feel" for the weld parameter values that gave the strongest welds. For the membrane-to-ring welds, the primary variables of interest were the percentage of current, the voltage, the clamping force, and weld speed. Each of the parameters was varied systematically to find the optimum setting. Each test was performed three times at each weld parameter setting to check for repeatability. The optimum set of parameters was determined for the membrane-to-ring welds. Under the optimum parameters settings, the average stress at failure was 111,644 psi. The minimum yield strength of the membrane material is 120,000 psi. Therefore, the ring-to-membrane welds have strength nearly equal to the yield strength of the parent material. In nearly all of the samples, the weld failures were all along the edge of the welds, indicating that the necking or annealing of the material near the weld, and not weakness of the weld itself, was the cause of failure.

Membrane-to-membrane weld tests were also completed under this activity. SAIC had previously welded large areas of 3-mil half-hard stainless steel under a heliostat fabrication contract. [1] The high stresses in the dish facet required that the welding parameters be optimized for maximum strength. Again, the parameters listed in **Table 4.1-2** were varied and the optimum values identified.

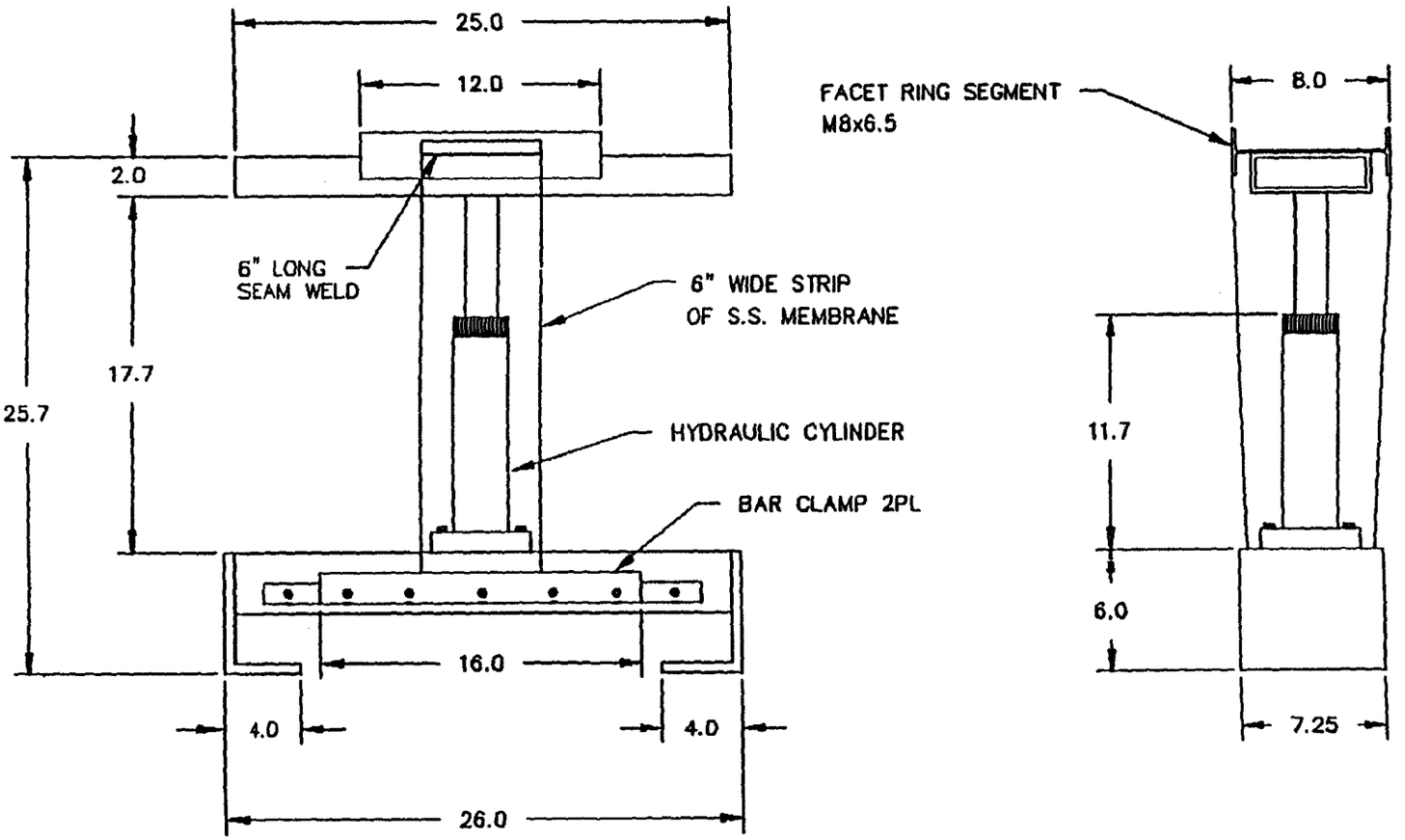

Figure 4.1-1. Hydraulic Membrane Test Apparatus

As was the case in previous membrane-to-membrane tests, the welds were found to be stronger than the parent material. All failures occurred in the membrane at significant distance away from the welds. The average stress at yield for the membrane-to-membrane weld tests was 133,000 psi. The stress at failure is difficult to determine with this type of test because of the rapid transition from yield to ultimate failure.

The weld tests were successful in determining the optimum parameters for the membrane-to-ring weld and the membrane-to-membrane welds. The factor of safety to failure for the membrane-to-ring welds is 1.3 and for the membrane-to-membrane welds it is 1.5. Therefore, the welding techniques applied to the facet fabrication process are adequate.

4.2 Laser Ray Trace Optical Testing

To have a method for determining the optical quality of the facets fabricated in this project, SAIC developed a simple, yet effective, concentrator optical test system. A sketch of the system is shown in **Figure 4.2-1**. A laser and a target are located at a distance corresponding to the center of curvature of the dish/facet. The laser is mounted in such a way that it's beam can be rotated to sweep across the surface of the facet from the center of curvature. If the facet were a perfect sphere, the image of the laser would be reflected off the dish back to the same spot. However, any error in the surface slope will cause the image dot to be displaced. For a 10 meter focal length facet, a calculation of the sensitivity of the system shows that a 1 mrad error in the surface slope (compared to a sphere) would result in a 4-cm displacement of the image dot. This simple test is therefore sensitive and adequate for characterizing the surface of long focal length dish facets. A photograph of this system is shown in **Figure 4.2-2.**

Data is taken with the laser ray-trace apparatus by aiming the laser at discrete points on the dish. The aim point is noted, as well as the position of the reflected ray on the target. **Figure 4.2-3** shows the system in use. In the figure, the beam reflected off the mirror facet is visible about 3-cm below and the to left of the center of the target. This procedure is repeated for many points on the surface of the dish. A FORTRAN program was written (LARRY - for LAserR RaY trace) to process the data obtained from this test. An outline of the analysis procedure follows:

1. The distance from the laser to the center of the dish is input. This value is taken to be the radius of curvature of the spherical shell, and twice the focal length of the parabolic shape against which the actual surface will be compared.
2. For each data point, four values are input to the code: the azimuth and elevation angles of the incident ray, alpha and beta, respectively, and the position of the reflected spot on the target, in polar coordinates, i.e., r and theta.
3. These inputs are used to calculate the following vectors and positions in space:
   - $\underline{i}$ the direction of the incident laser ray (from alpha and beta);
   - p the point of intersection of the incident ray with the spherical shell (from i and R);
   - $\underline{s}$ the surface normal direction of the sphere at the point p (from i);
   - a the intersection of the incident ray with the parabolic shell (from i and R);
   - $\underline{n}$ the surface normal of the parabolic shell at the point a (from a and R);
   - d the position of the reflected spot (from r, theta, alpha, and beta);
   - $\underline{r}$ the direction of the reflected ray (from p and d); and
   - $\underline{x}$ the calculated normal vector to the surface being measured (from s and r).
4. Once the normal to the surface ($\underline{x}$) has been determined, the cross-products of that calculated surface normal with those of the spherical shell ($\underline{s}$) and the parabolic shell ($\underline{n}$) are calculated. Since the magnitude of the cross-product vector is the sine of the angle between two unit vectors, this determines the angular slope error of the surface relative to each of those surfaces. The resulting angles phi (error angle relative to the parabola) and omega (error angle relative the spherical shell) are then averaged over the surface.

Optical testing was performed on both of the SAIC prototype facets at SAIC's laboratories and at SERI. The test results from the first facet tested at SAIC are shown in **Figure 4.2-4**. A single transverse sweep was performed in a direction perpendicular to the weld seams in the membrane. This test was performed with the facet focused to a f/D of 2.72. Data points were taken in an area-averaged fashion across the facet. In the scale of the figure, the difference between the slope error relative to a sphere and relative to a parabola are indistinguishable.

The results from the first facet show that errors of less than about 2 mrad are present up to about 1.2 meters in radius, and then the slope errors begin to increase sharply toward a peak of about 15

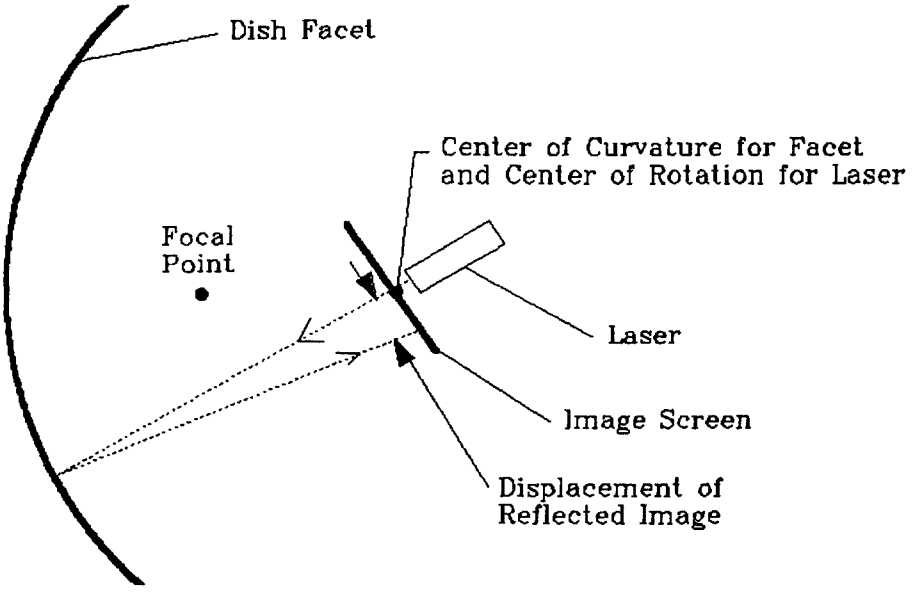

Figure 4.2-1. Concentrator Optical Test System Sketch

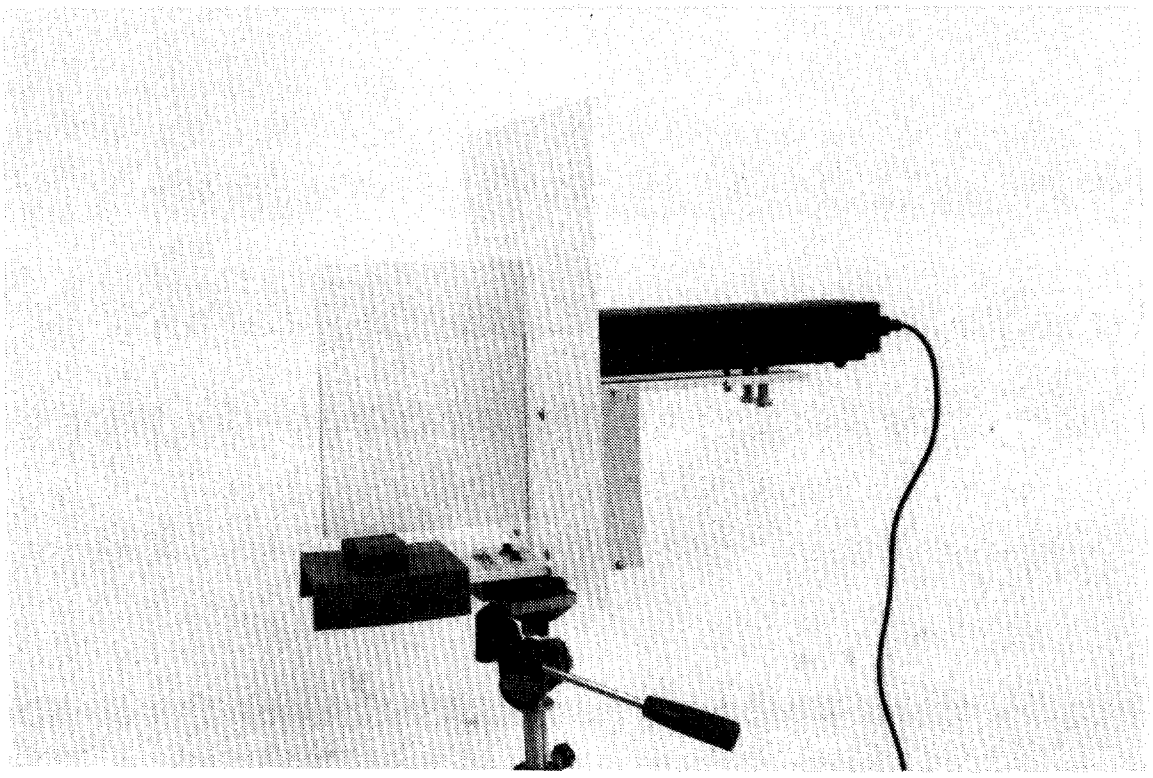

Figure 4.2-2. Concentrator Optical Test System

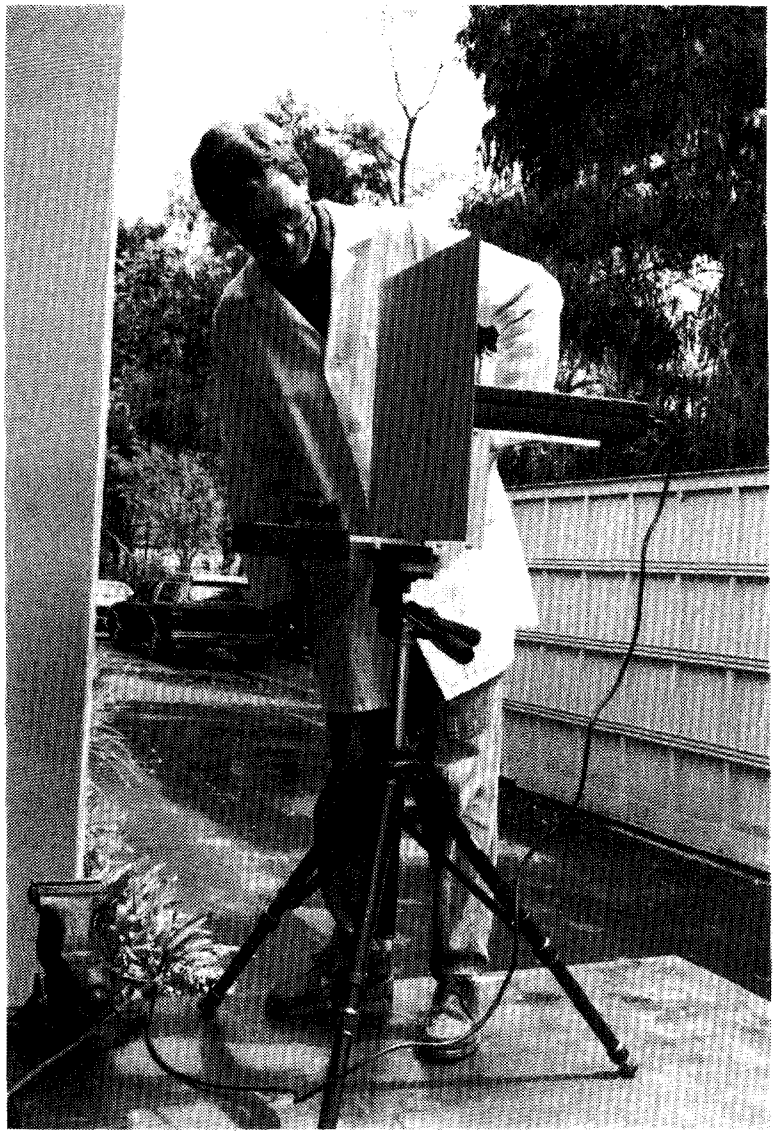

Figure 4.2-3. Optical Test System in Use

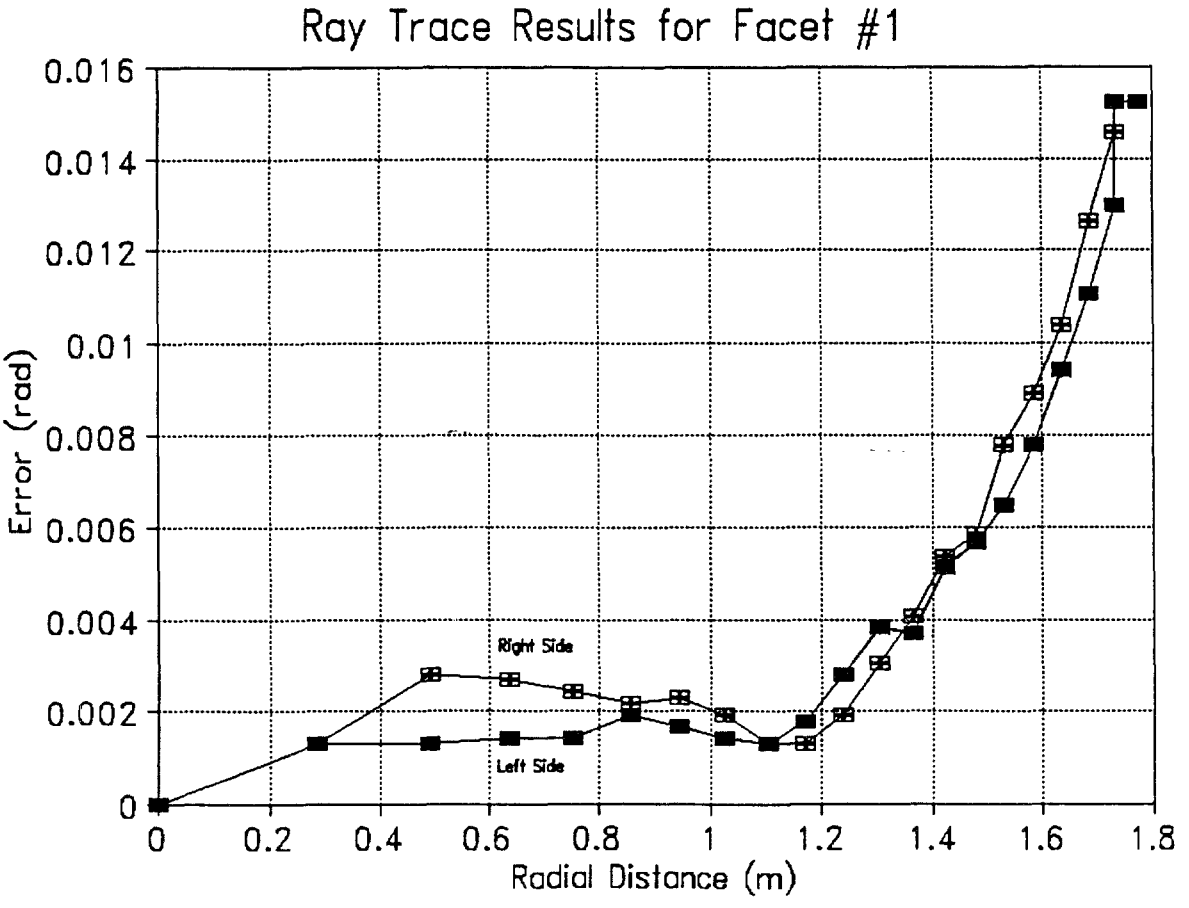

Figure 4.2-4. Optical Ray Trace Test Results of Facet #1

mrad at the edge of the module. An average slope error across the dish is about 5 mrad, based upon these measurements. The RMS slope error is 6.65 mrad.

Testing at SERI on the same facet showed a slope error of 3.3 mrad. The better results from SERI's test are due to the fact that the focal length of the mirror as tested at SAIC was not optimized for the position of the laser ray trace system. This effect would cause a general shift in the Y direction of the curve shown in **Figure 4.2-4**, resulting in a higher overall slope error.

Similar optical testing was also performed on the second facet fabricated by SAIC. The membrane pretension was increased in the second facet to obtain a better overall facet shape. The higher membrane pretension reduced the slope error as shown in **Figure 4.2-5**. The higher membrane pretension acted to reduce the slope error near the edges significantly, as predicted. In tests performed at SERI, SAIC's facet design was shown to have an equivalent RMS slope error of between 2.5 and 2.8 mrad, including specularity. These results are within the optical quality requirements set forth at the beginning of the project, i.e., less than 3.0 mrad overall (including film specularity) slope error.

Improvements in the membrane material flatness received from our supplier for future fabrication efforts should provide some additional improvement in optical quality. The issue of membrane material quality control is addressed in Section 5.0 - Facet Fabrication.

4.3 Strain Cycling Test

Early in the project, concerns were raised about the effect of the daily focus/defocus cycling of the elastic membrane deformation concept. It was feared that the strain cycling would cause micro-cracking of the silver reflective layer, delamination, or otherwise adversely affect the performance of the reflective surface. Therefore, testing was initiated to evaluate the effect of cyclic bi-axial stress on stainless steel membranes when laminated with ECP 305 reflective film. Stress cycling on small coupon samples was also accomplished as a SERI activity in conjunction with this program. To form a basis for comparison, two membranes were laminated with identical fabrication procedures. The reflectivity of both samples were measured initially using a Devices & Services (D&S) Reflectometer which uses a red LED for the light source. Reflectivity of both samples ranged from 95.9% - 98.5%.

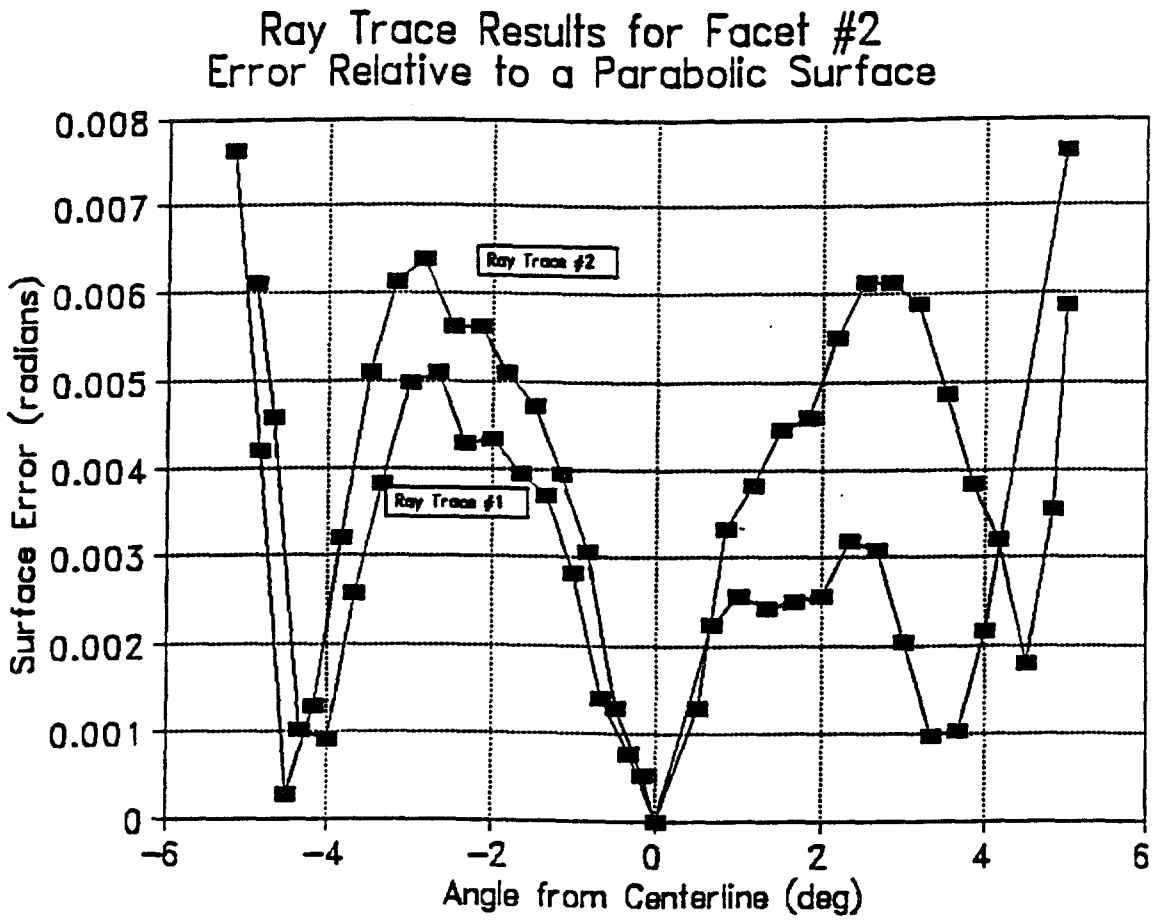

Figure 4.2-5. Optical Ray Trace Test Results of Facet #2

To perform a fatigue test on the film, a test apparatus was fabricated to simulate an actual faceted dish. Two 1.75-m (69-in) diameter rings were stacked on top of each other, the bottom was covered with a 1/4-in steel plate and the pieces were welded together. A membrane was stretched over the top of the rings and was pretensioned to 195 MPa (28,300 psi) using a tensioning bladder and tensioning strips. The test apparatus is shown in **Figure 4.3-1** and **Figure 4.3-2**. The pretension level was measured using strain gages attached to the membrane. Following pretension, the membranes were welded to the rings using our standard hand-held roll-resistance welding process. Then the bladder pressure was released. The final membrane stress, measured using the strain gages attached to the membrane as shown in **Figure 4.3-3**, was 2150 MPa (21,700 psi). This is close to the stress pretension level used in the second prototype facet.

Using a vacuum pump connected to a timer, the membrane was cycled from a flat condition to the desired membrane center deflection of 1.5-in, giving a maximum stress of 575 MPa (83,400 psi). The test apparatus was then cycled 610 times with about one hour required for each cycle. This corresponds to about 1-2/3 years of daily operation, or almost 2-1/2 years of 5-day-per-week operation.

In this experiment, strain gages were applied in pairs (1 radially, and 1 circumferentially) at four locations on the membrane, for a total of eight gages. There was good correlation between the readings from the radial gages with a maximum difference of 11.7% between the highest and lowest readings, as shown in **Figure 4.3-4**. The circumferential gages had a maximum difference of 43.8% as shown in **Figure 4.3-5**, with a spread probably due to misalignment during application and the effect of seams weld in the membrane. To obtain accurate strain gage readings, experiments were performed prior to the application of the strain gage to the membrane to determine the reinforcement effect of the strain gage itself and the glue used to adhere the strain gage to the membrane. The reinforcement effect of the gage was found to be 9 kPa (1,300 psi).

Reflectance measurements were made on the membrane before and after cycling. The locations of reflectivity measurements made on the test membrane are numbered 1 through 3 on **Figure 4.3-6**. A D&S Reflectometer was used to measure the reflectance of the reflective surface, as shown in **Figure 4.3-7**. **Figure 4.3-8** shows the individual measurements, and **Figure 4.3-9** shows the averages

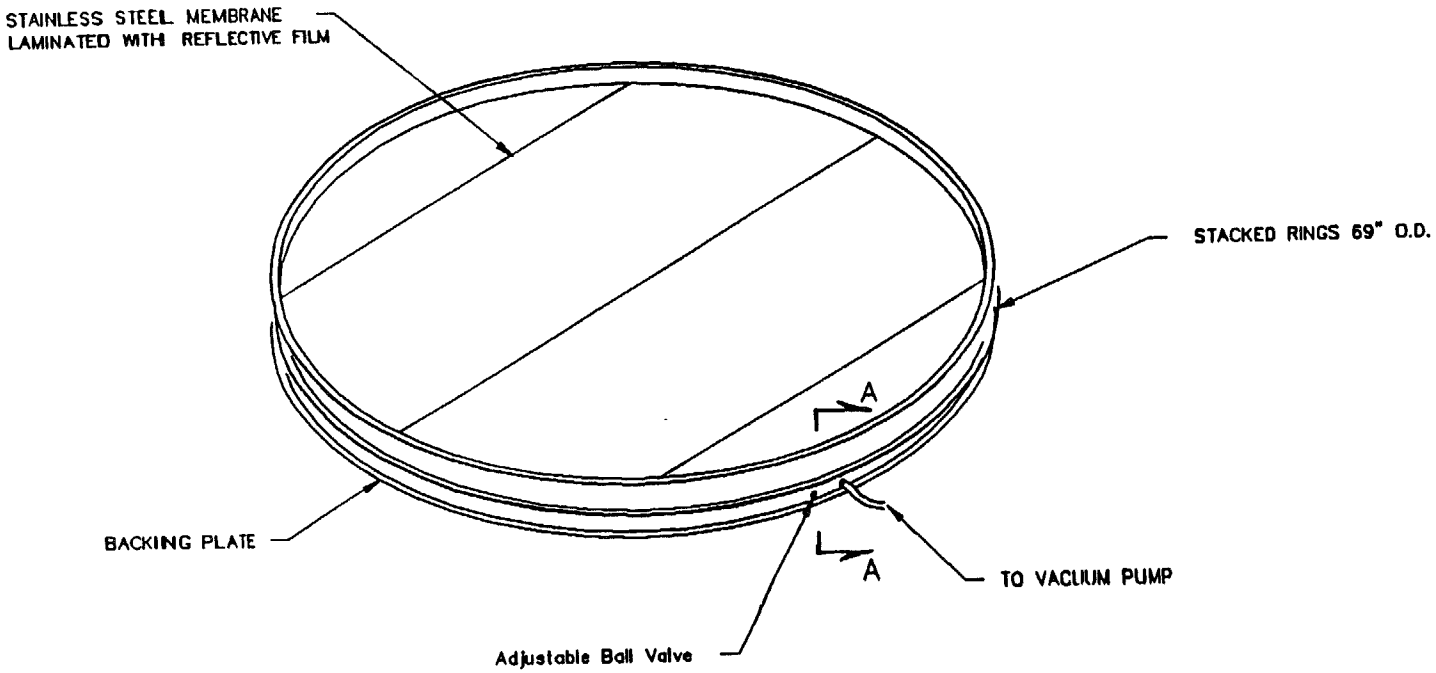

Figure 4.3-1. Strain Loading Test Apparatus

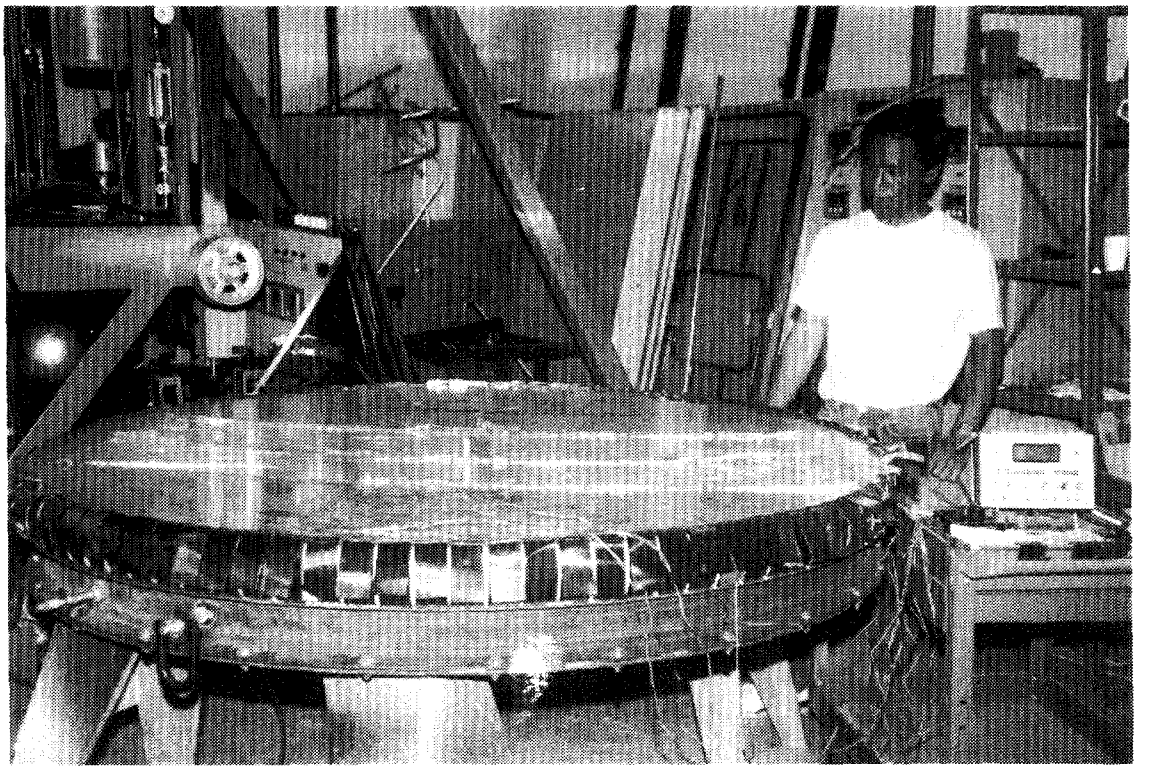

Figure 4.3-2. Photograph of Strain Cycling Test Apparatus

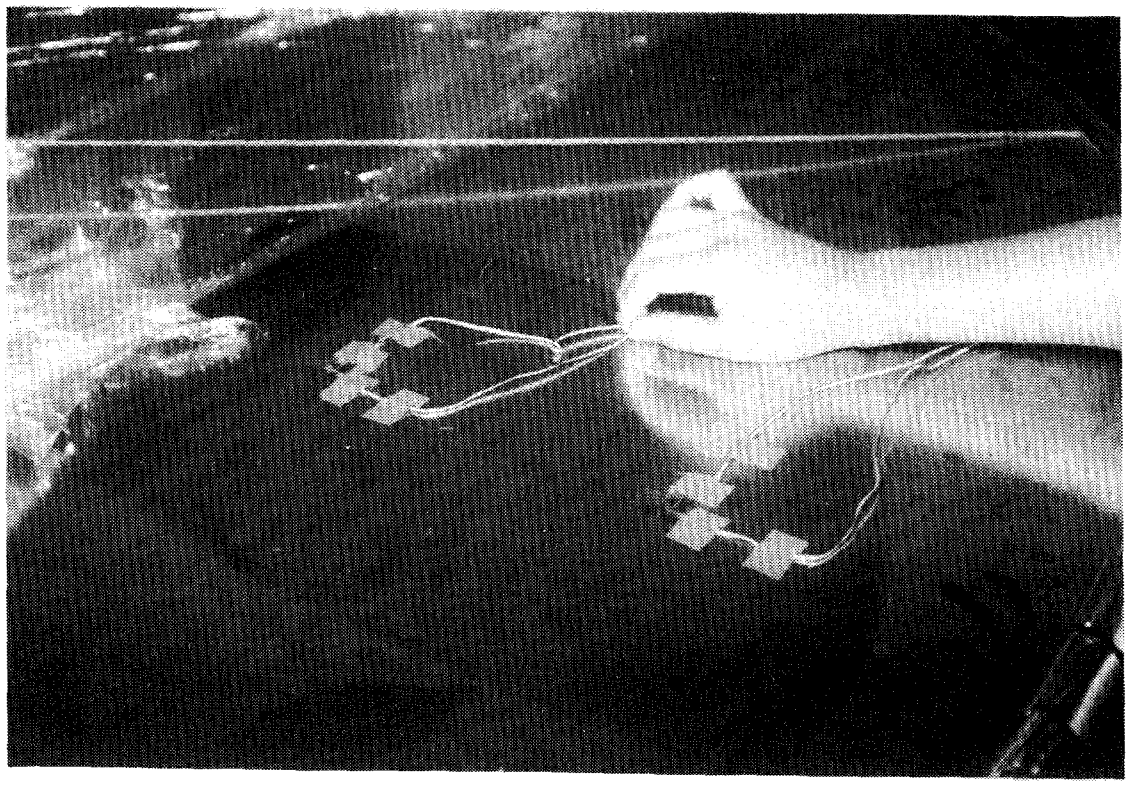

Figure 4.3-3. Attachment of Strain Gages to Strain Cycling Test Membrane

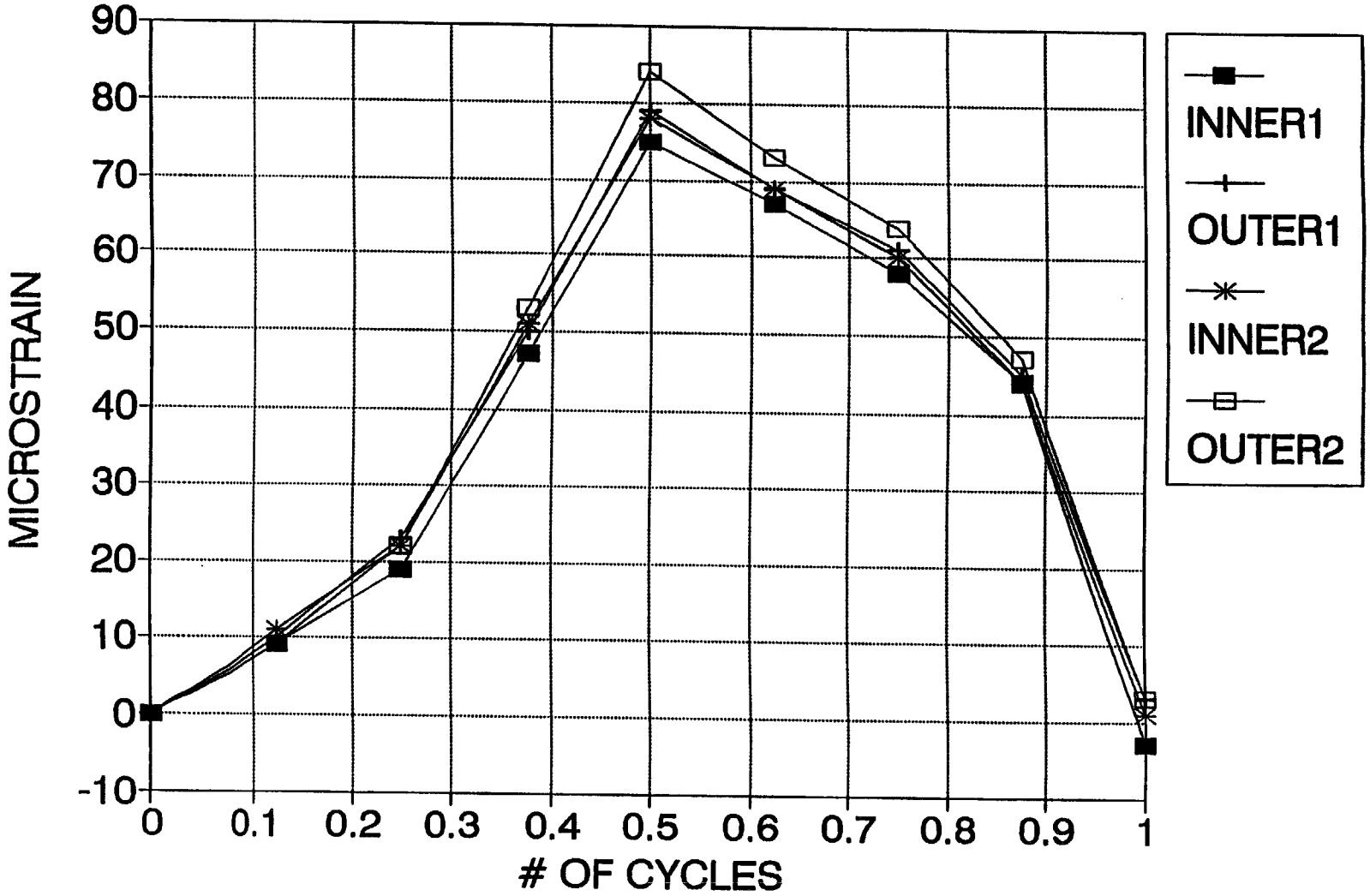

Figure 4.3-4. Radial Membrane Strain

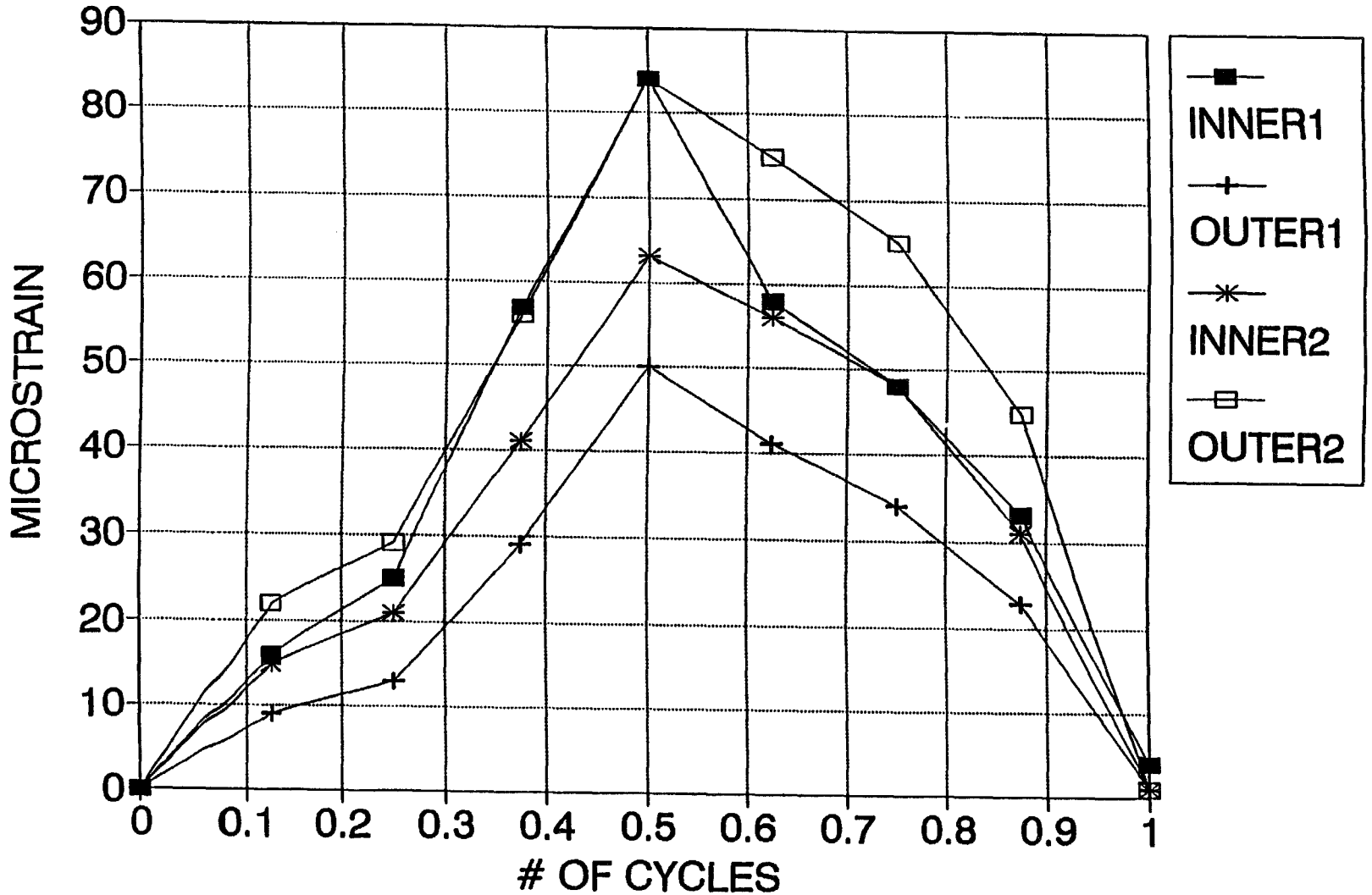

Figure 4.3-5. Circumferential Membrane Strain

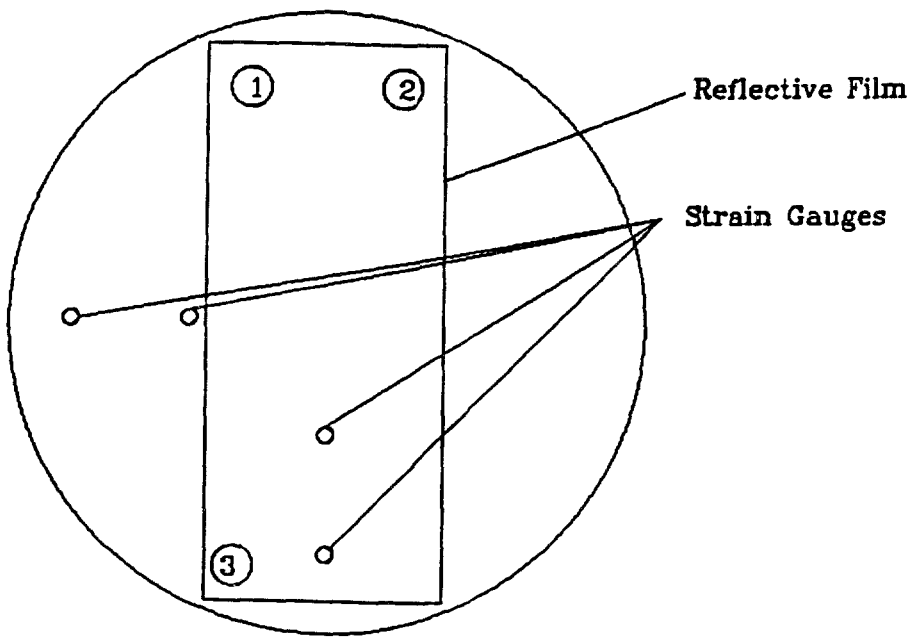

Figure 4.3-6. Location of Reflectivity Measurements on Test Apparatus

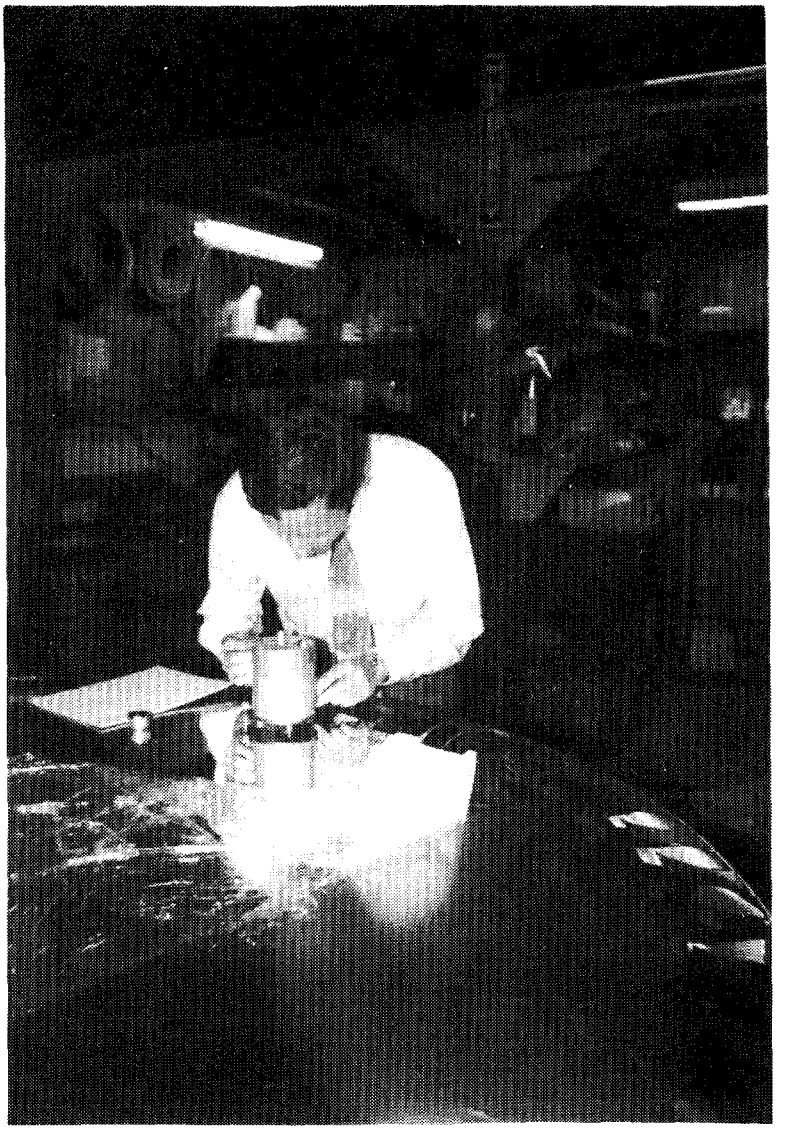

Figure 4.3-7. Reflectance Measurement Using D&S Reflectometer

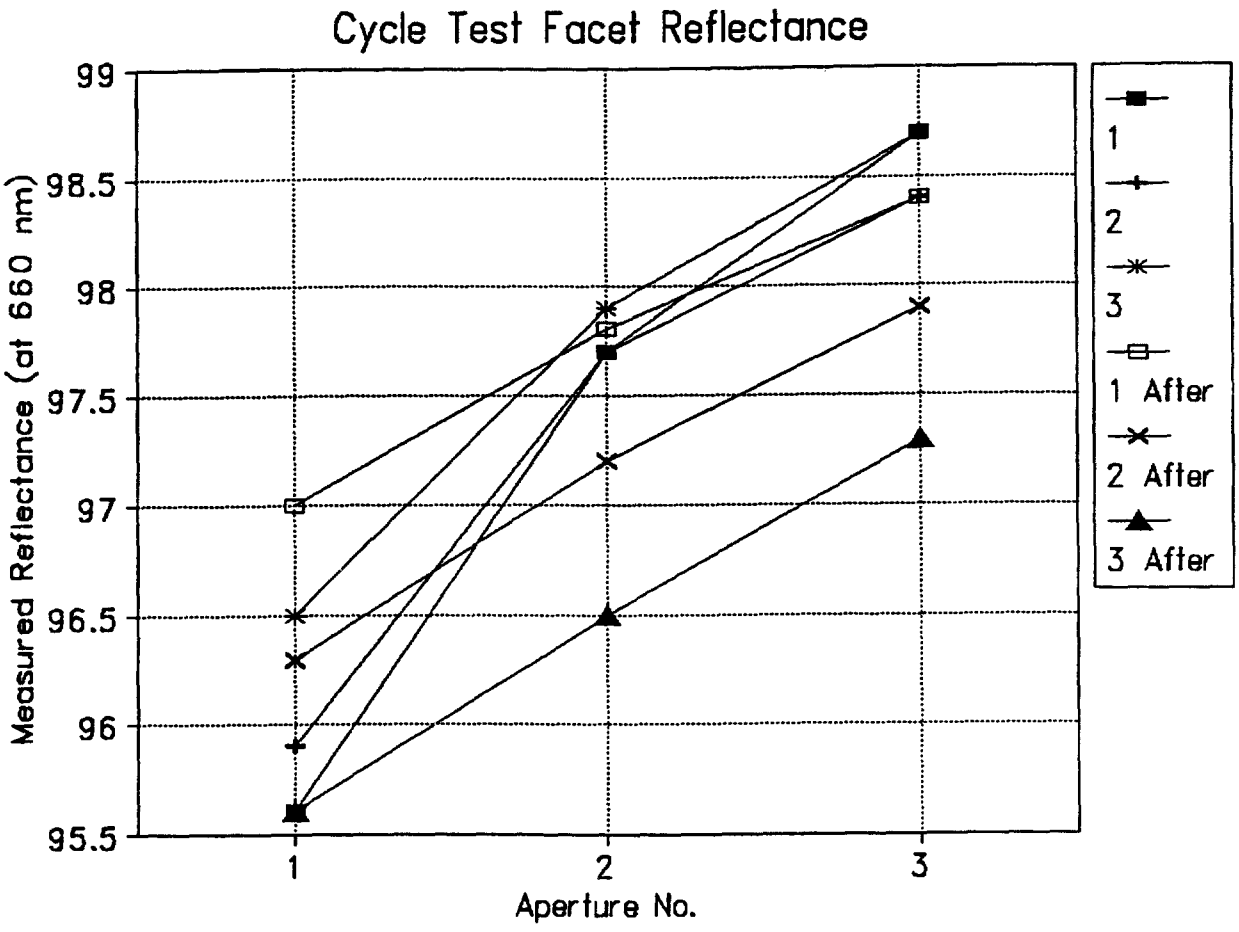

Figure 4.3-8. Individual Reflectance Measurements on Strain Cycling

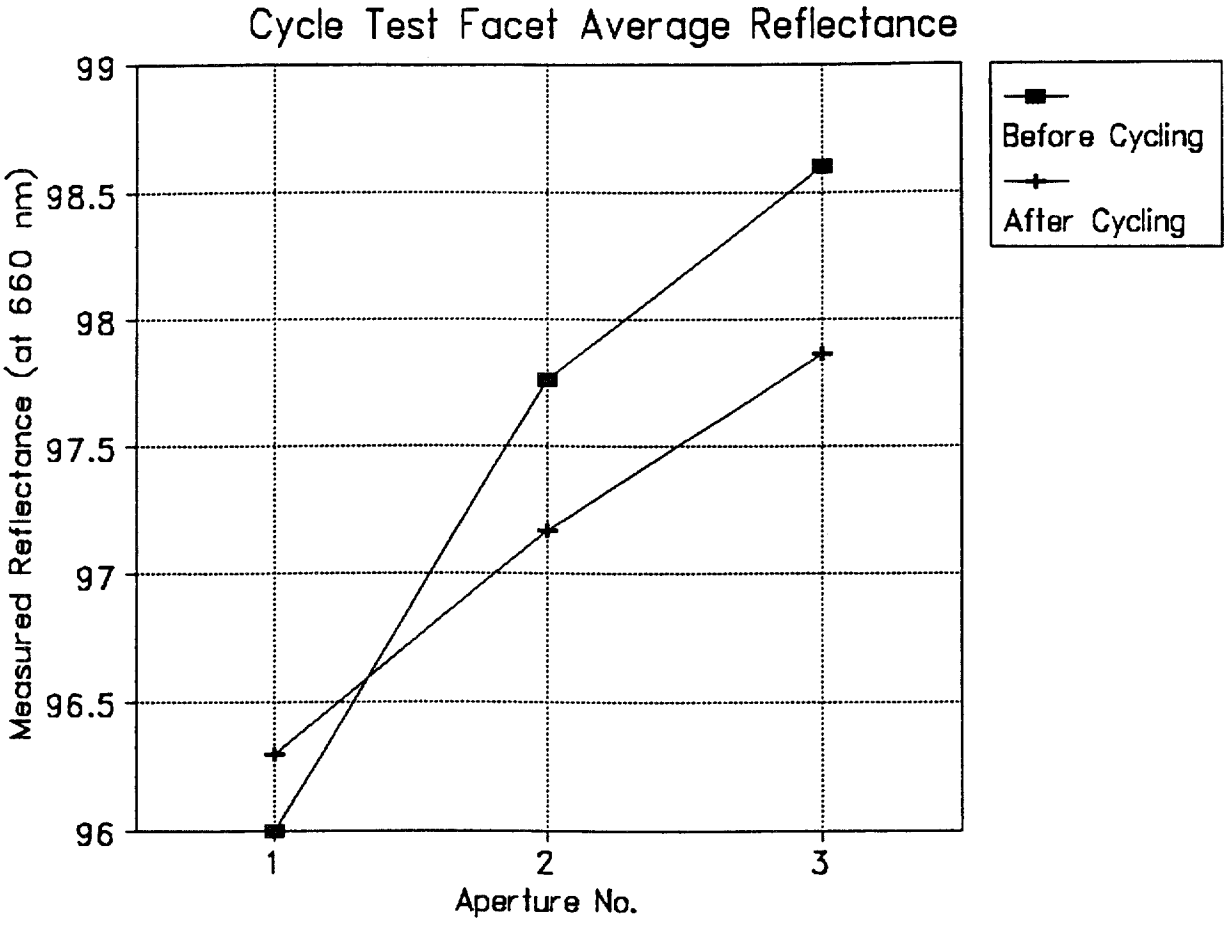

Figure 4.3-9. Averaged Reflectance Measurement on Strain Cycling Test Apparatus

of the measurements made before and after cycling. The results are shown in tabular form in **Table 4.3-1.**

Table 4.3-1. Reflectance Measurement Results From Axial Cycling Tests

	Aperture		
Before Cycling	1	2	3
Location 1	95.4	97.5	98.5
Calibration	83.9	84.3	84.7
Location 2	95.8	97.6	98.3
Calibration	84.0	84.4	84.8
Location 3	96.5	97.9	98.7
Calibration	84.0	84.5	84.8
After Cycling			
Location 1	96.9	97.7	98.3
Calibration	84.0	84.4	84.8
Location 2	96.3	97.2	97.9
Calibration	84.1	84.5	84.8
Location 3	95.6	96.5	97.3
Calibration	84.1	84.5	84.8
Adjusted to 84.5% at Aperture 2			
Before Cycling			
Location 1	95.6	97.7	98.7
Location 2	95.9	97.7	98.4
Location 3	96.5	97.9	98.7
Average	96.0	97.8	98.6
After Cycling			
Location 1	97.0	97.8	98.4
Location 2	96.3	97.2	97.9
Location 3	95.6	96.5	97.3
Average	96.3	97.2	97.9

At the smallest aperture (#1) in **Figure 4.3-8**, the difference between the average reflectance before and after cycling is within the scatter of the individual measurements before cycling. At the larger apertures, the average reflectance is seen to have decreased slightly after cycling. The difference is not large however, and is almost within the scatter between individual measurements. The effect may be due simply to the cleanliness of the film at the time of the initial measurements as compared to

the same film after testing was completed. The film was also examined under a microscope and no micro-cracks were observed. The results from the axial cycling tests conducted by SERI corroborated these results.

5.0 FACET FABRICATION

The first- and second-generation prototype mirror facets were fabricated at SAIC's Energy Projects Division Laboratories located in San Diego, CA. The facets were fabricated using the techniques and tooling described earlier in this report.

The two facet fabrication processes considered most critical are the membrane welding process and the membrane tensioning and attachment process. A sketch and photograph of the prototype membrane welding process is shown in **Figure 5.0-1**. The 61-cm by 9.1-m (24-in wide by 30-ft long) strips of .0762-mm (.003-in) thick stainless steel foil are first tack welded together at 2.5-cm (1-in) intervals while on the 1.22-m by 9.1-m (4-ft by 30-ft) membrane vacuum table. The definition of the flatness of the membrane is determined during the tack-welding process. This process is analogous to pinning a garment before it is sewn. The membranes are also laminated with ECP-305 reflective film at this time using a dry lamination process. As the membrane strips are tack welded, the membrane is rolled onto a 23-cm (9-in) diameter roll as shown in the figure. The membrane is then routed through the roll-resistance weld heads and rolled onto a second 23-cm (9-in) diameter roller. The continuous roll-resistance seam welds are then executed by moving the roller-support carriage, as shown in **Figure 5.0-2**. The correct weld parameters are critical to obtaining a high-quality weld. Critical parameters include the wheel width, wheel pressure, electric current, AC cycle time, and weld carriage speed. The stainless steel foil used for fabrication of the facets was received from the supplier with non-uniformities in its flatness. This was considered to be an anomaly since material that SAIC had previously received from the same supplier was very flat. The problem was traced to mis-adjustment of the flattening mill used at the supplier's plant. However, the non-uniform steel had to be used because new material could not be received in time to meet scheduled production. This caused some difficulty in welding and may have also affected optical quality of the facets.

The method used for tensioning the membrane in a low-production scenario is depicted in **Figure 5.0-3**. The tensioning method replicates the membrane tensioning device for the Commercial Manufacturing Scenario to the extent practically possible. The prototype tensioning fixture allows in-plane tensioning of the membrane and has provisions for circumferential expansion at the intermittent attachments to the tensioning device. These two issues are critical for providing uniform circumferential and radial tension in the membrane. The use of the air-inflated tensioning bladder

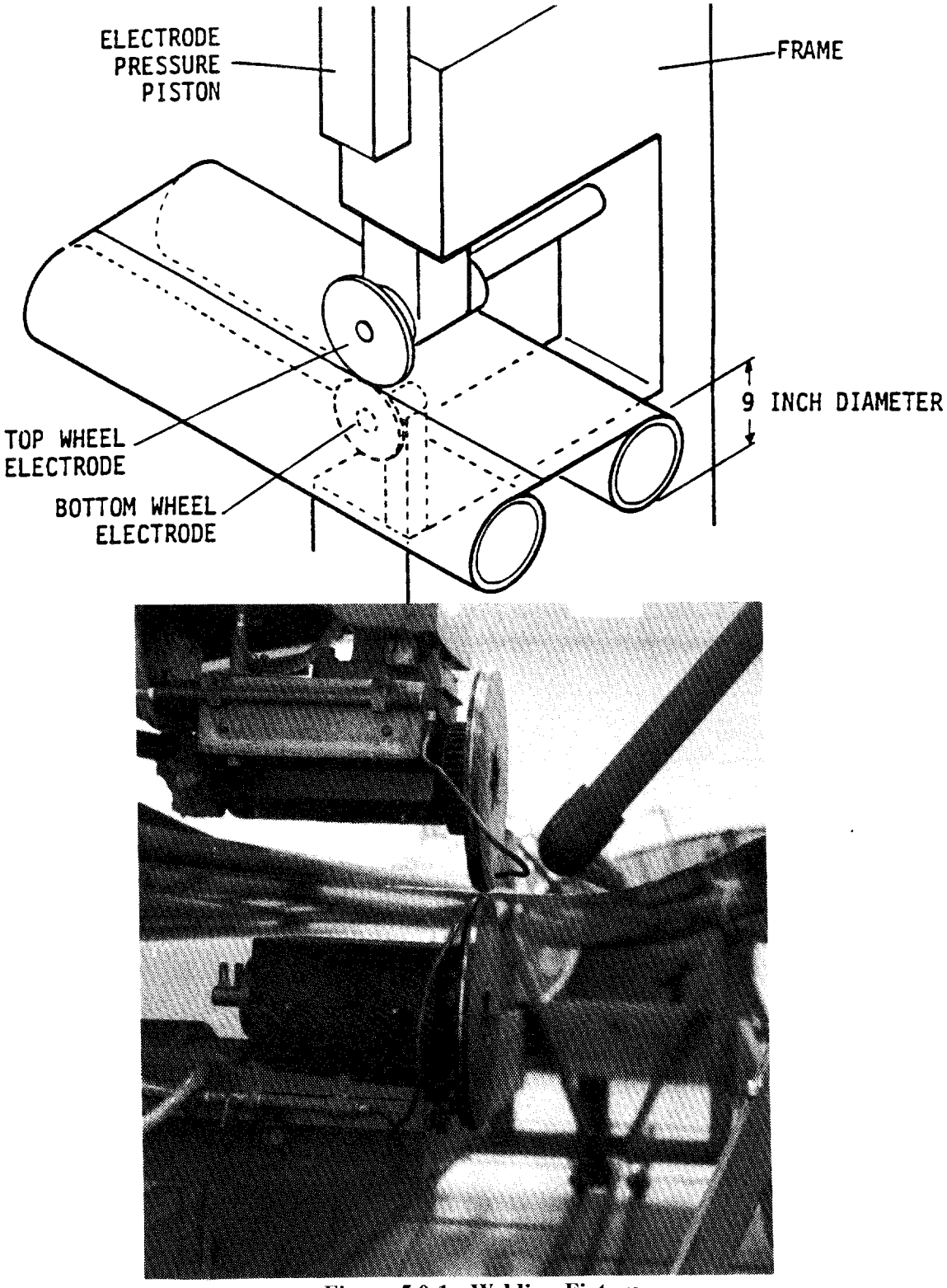

Figure 5.0-1. Welding Fixture

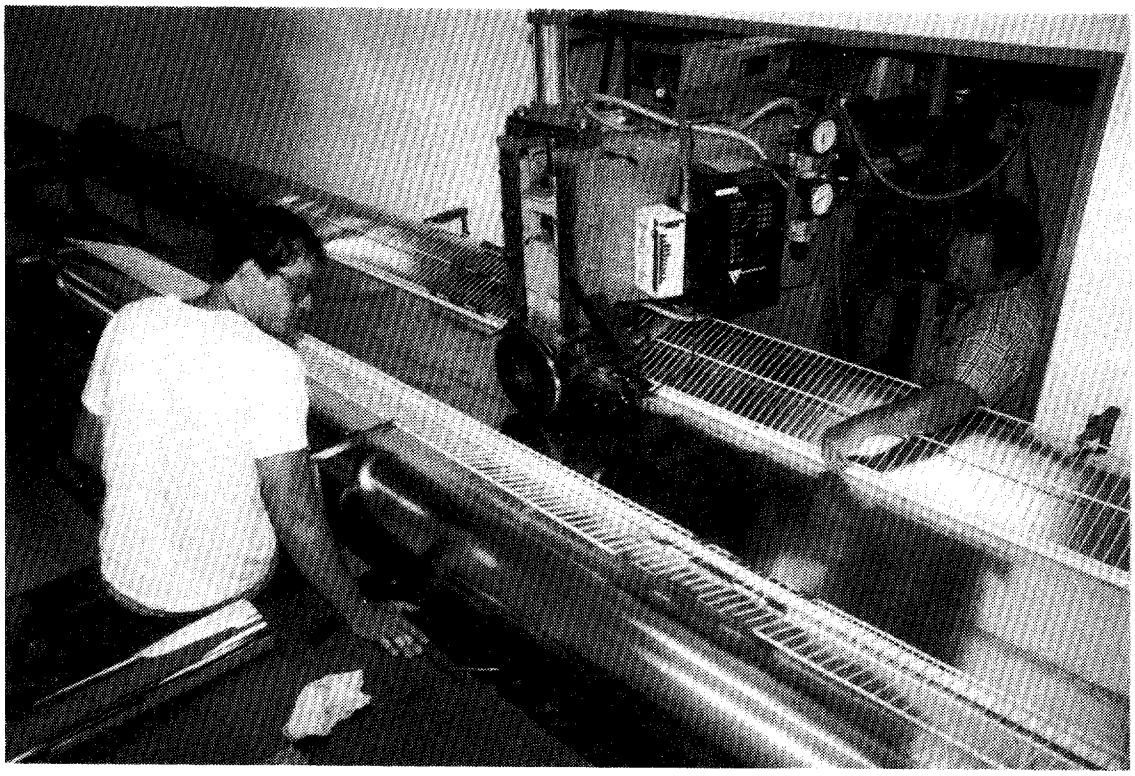

Figure 5.0-2. Membrane Welding

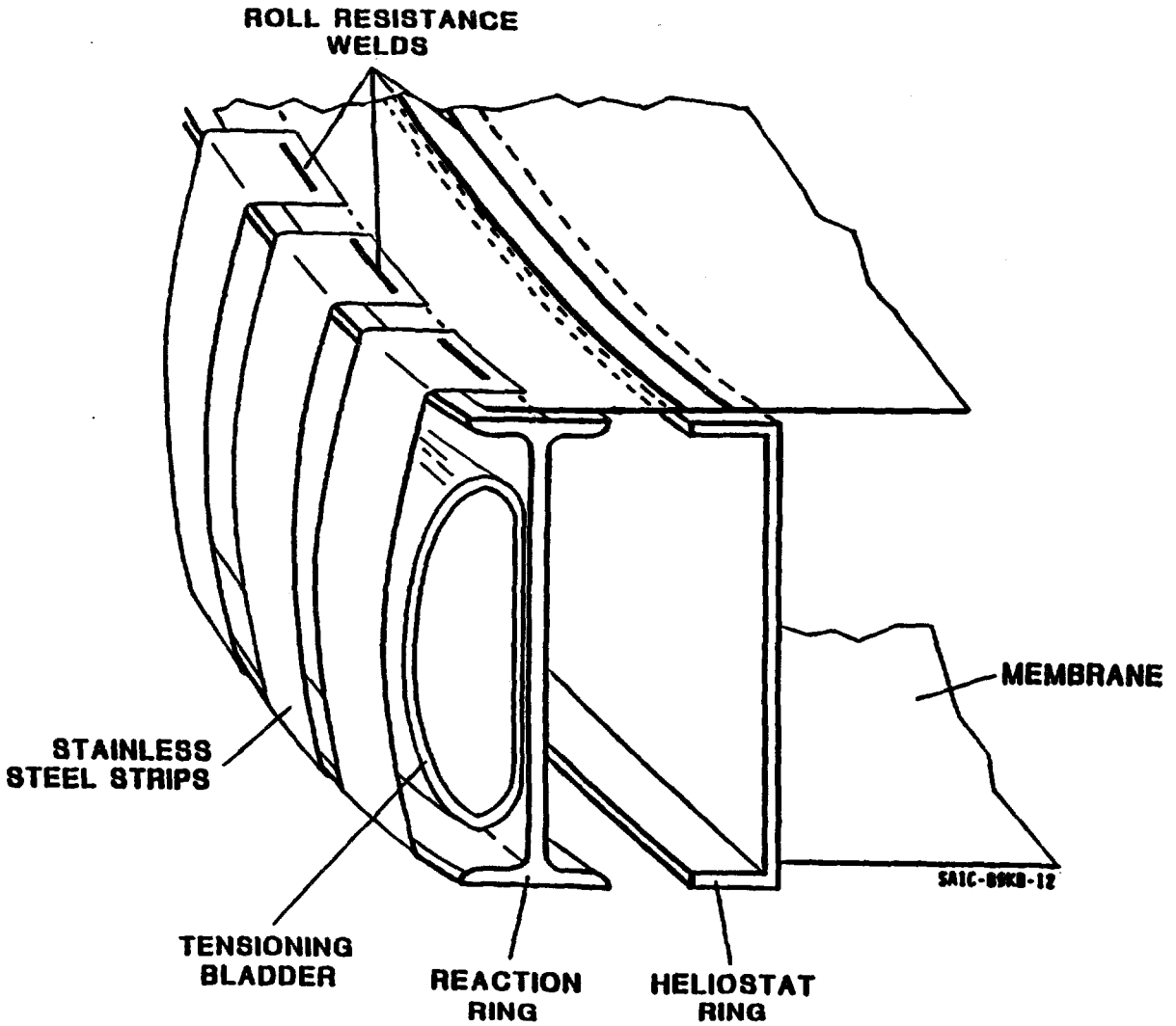

Figure 5.0-3. Membrane Tensioning Fixture

imparts uniform stress rather than uniform strain on the membrane; this is important because a uniform stress removes inconsistencies and wrinkles in the membrane.

As shown in **Figure 5.0-4**, a reaction ring is placed around the outside of the actual facet ring for prototype production. The reaction ring is in the form of a channel with the tensioning bladder on the outside of its web, as shown in **Figure 5.0-5**. Stainless steel foil strips are welded to the perimeter of the top and bottom membranes, as shown in **Figure 5.0-6**. The tensioning strips, attached to a 3-m diameter stretched membrane facet, are shown in **Figure 5.0-7**. The bladder is inflated pulling the strips radially and tensioning the membranes. The facet, after tensioning, is shown in **Figure 5.0-8**. Once the membranes are under tension, the hand-held roll-resistance welder is used to weld the membrane to the facet ring along the top and bottom flanges, shown in **Figure 5.0-9**. Once the membranes are welded to the ring, the bladder pressure is released and the tensioning strips, reaction ring, and excess membrane material are removed. Reflective ECP 244 tape is then used to cover the seam welds and edges of the reflective film. Installation of the focus control components inside the plenum completes the facet fabrication process. The completed facet is shown in **Figure 5.0-10**.

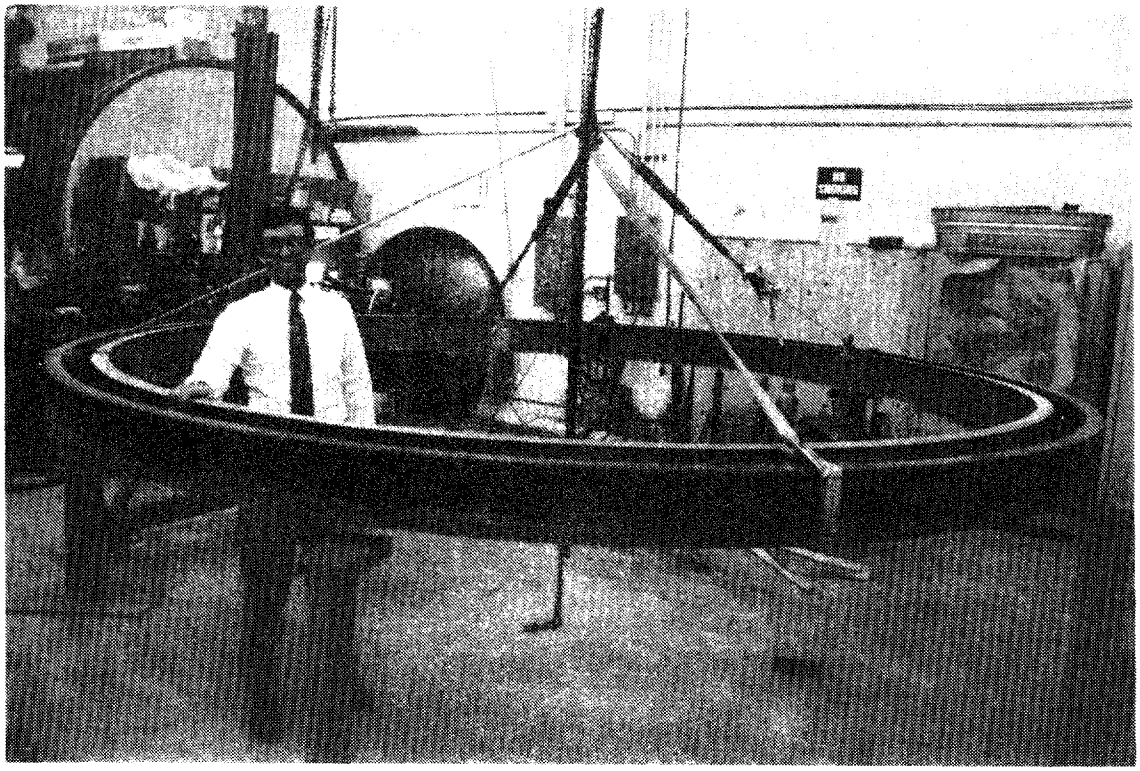

Figure 5.0-4 Facet Ring in Reaction Ring

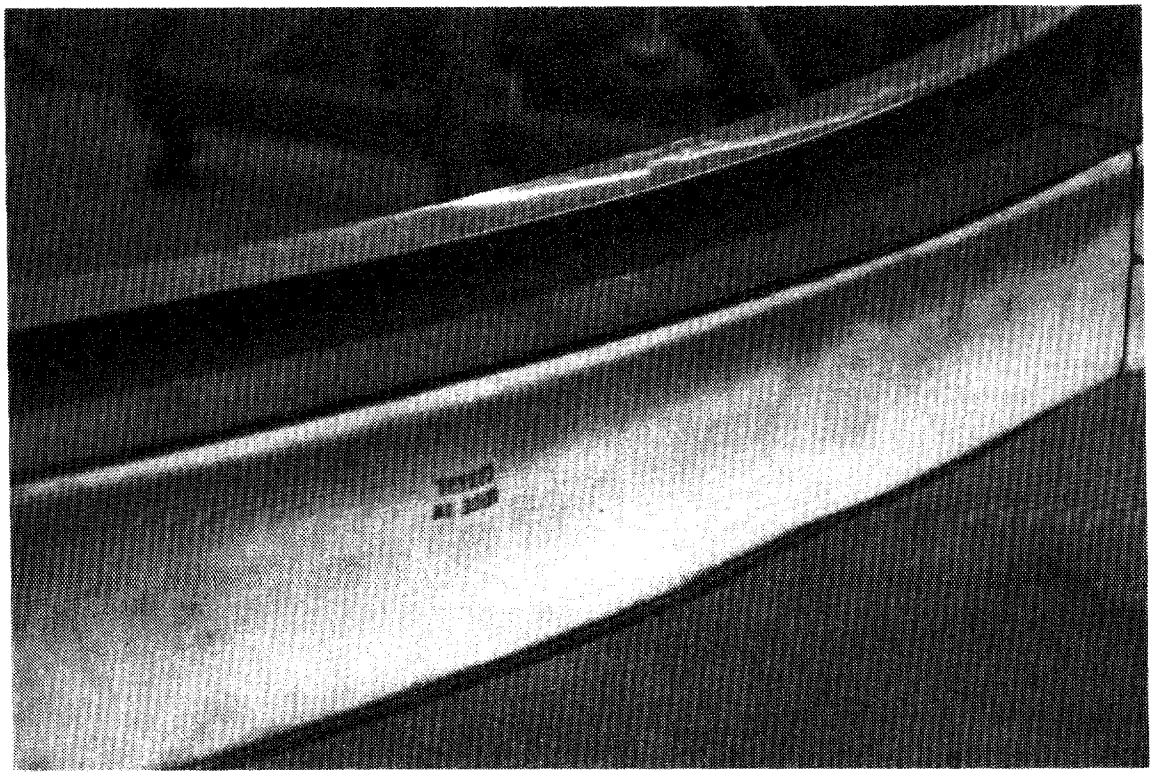

Figure 5.0-5 Tensioning Bladder in Reaction Ring

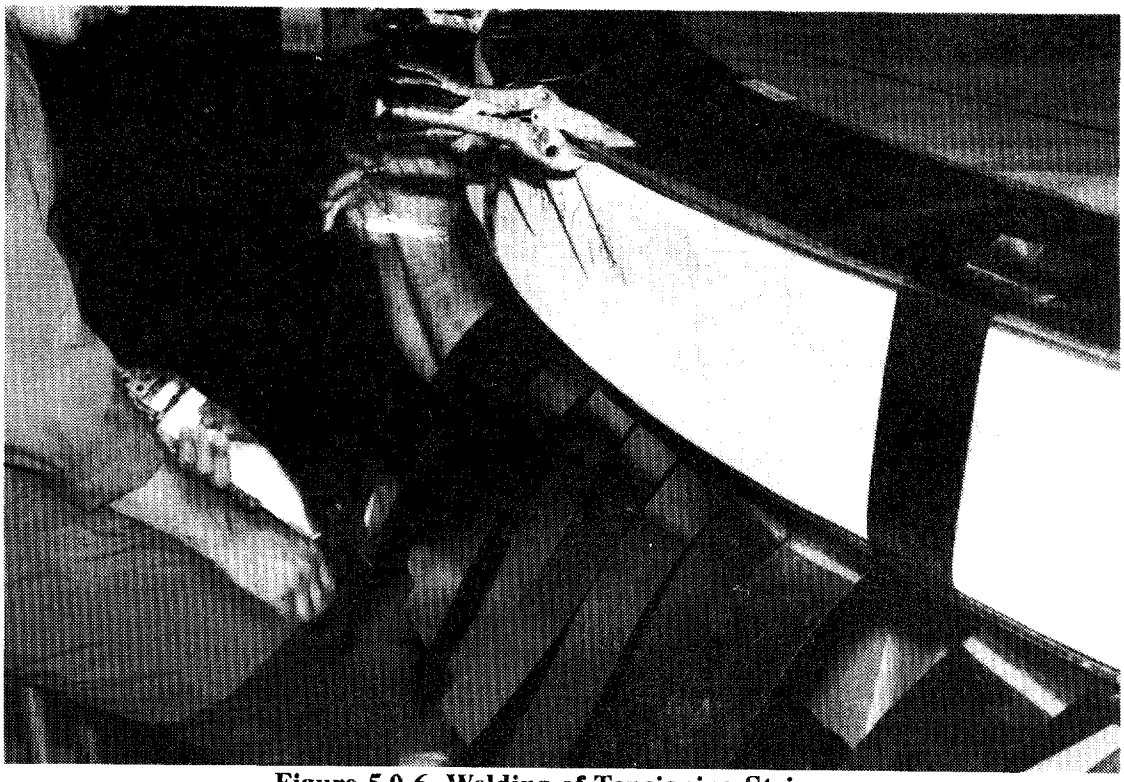

Figure 5.0-6 Welding of Tensioning Strips

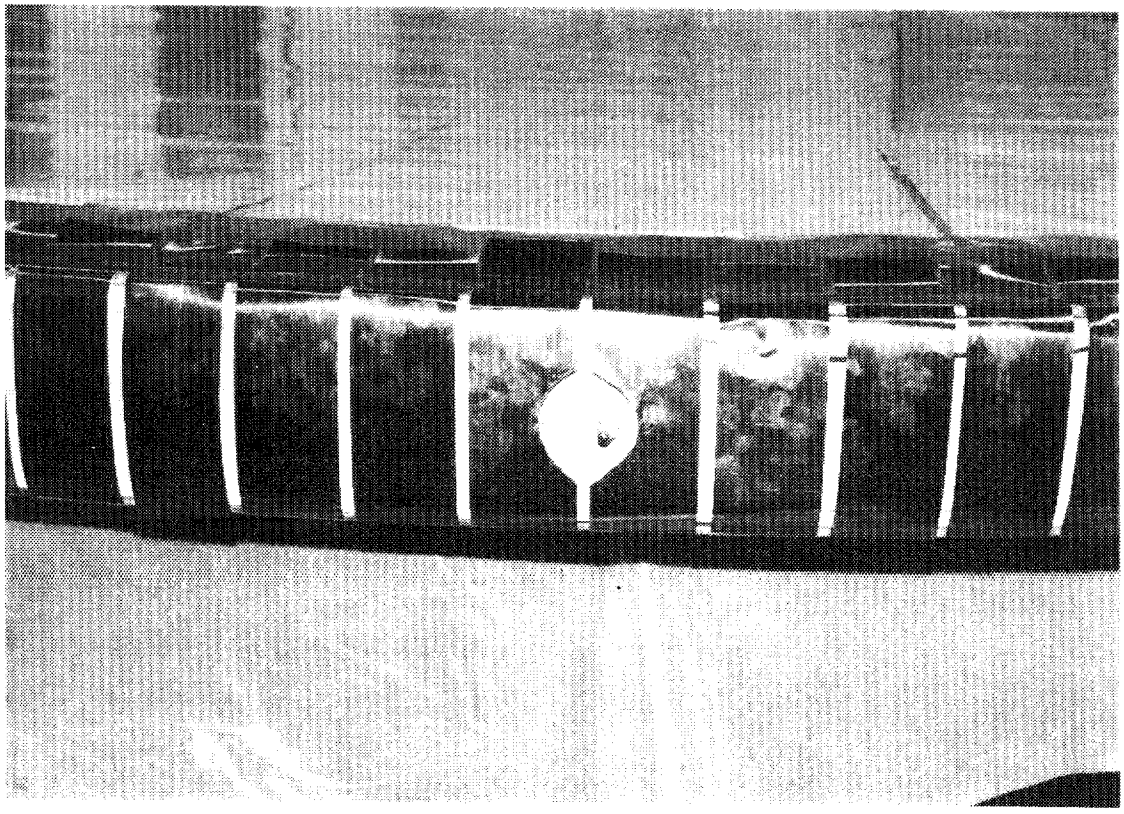

Figure 5.0-7 Welded Tensioning Strips

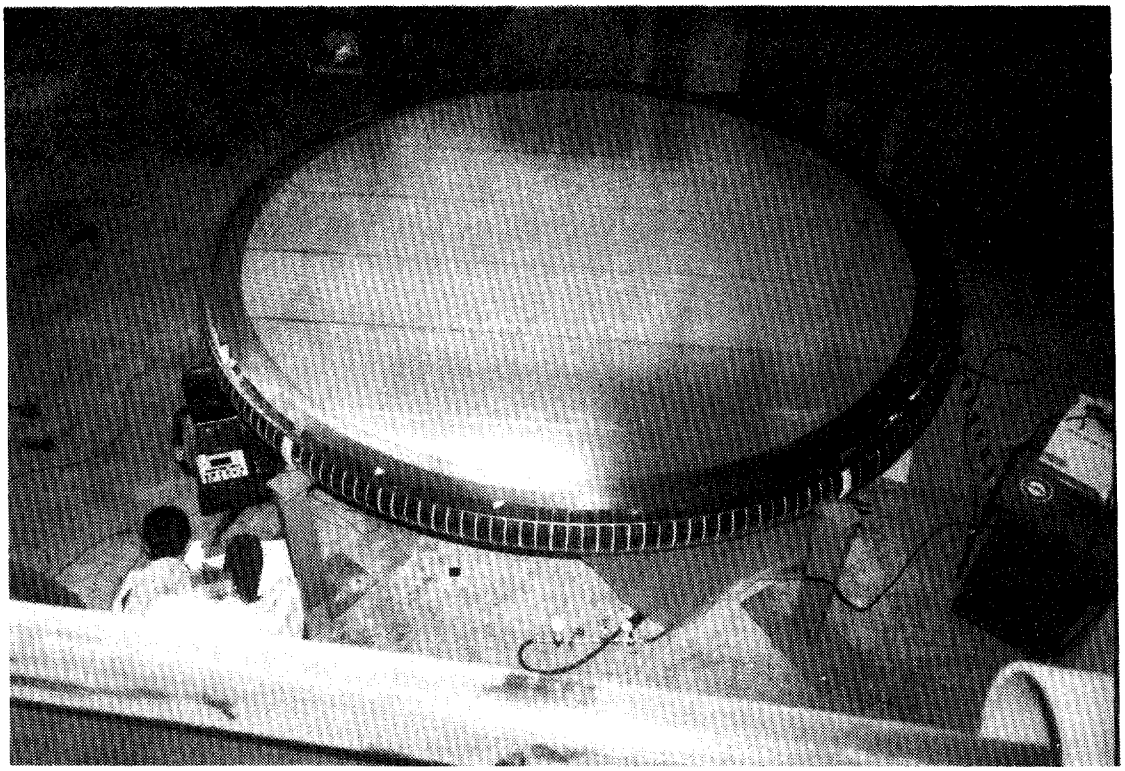

Figure 5.0-8 Tensioned Facet

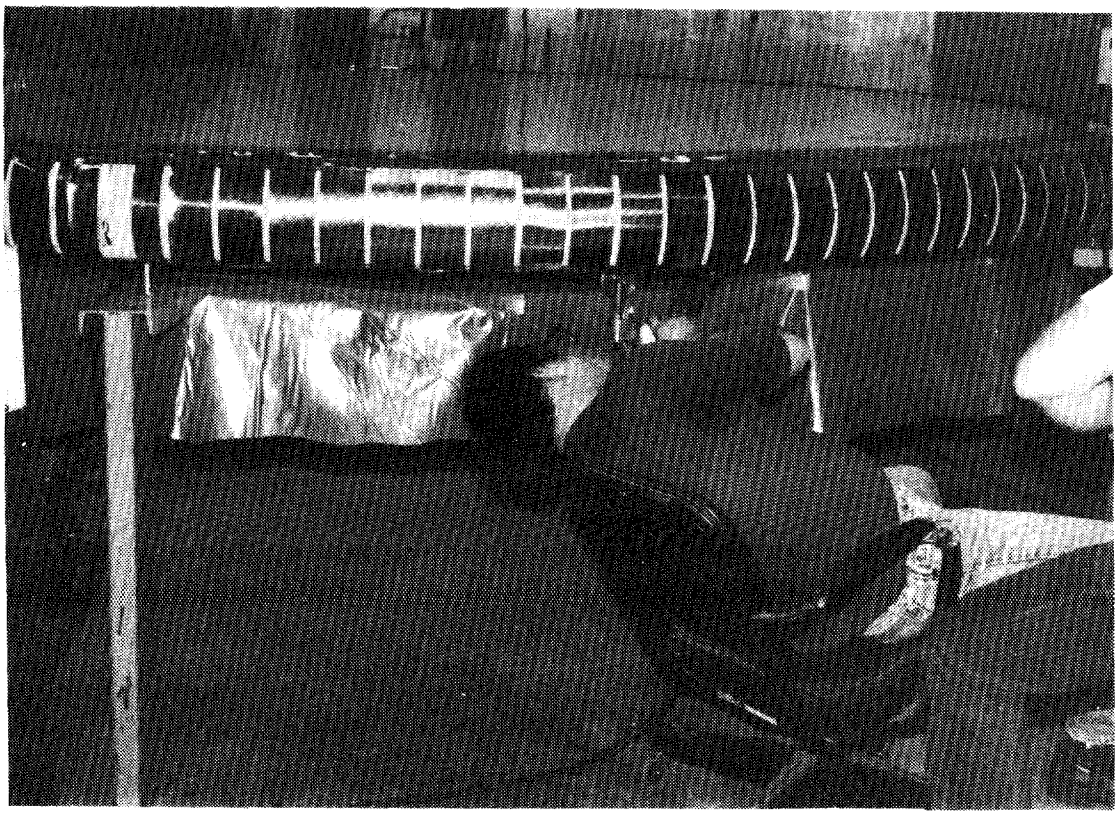

Figure 5.0-9 Welding Tensioned Membrane to Ring

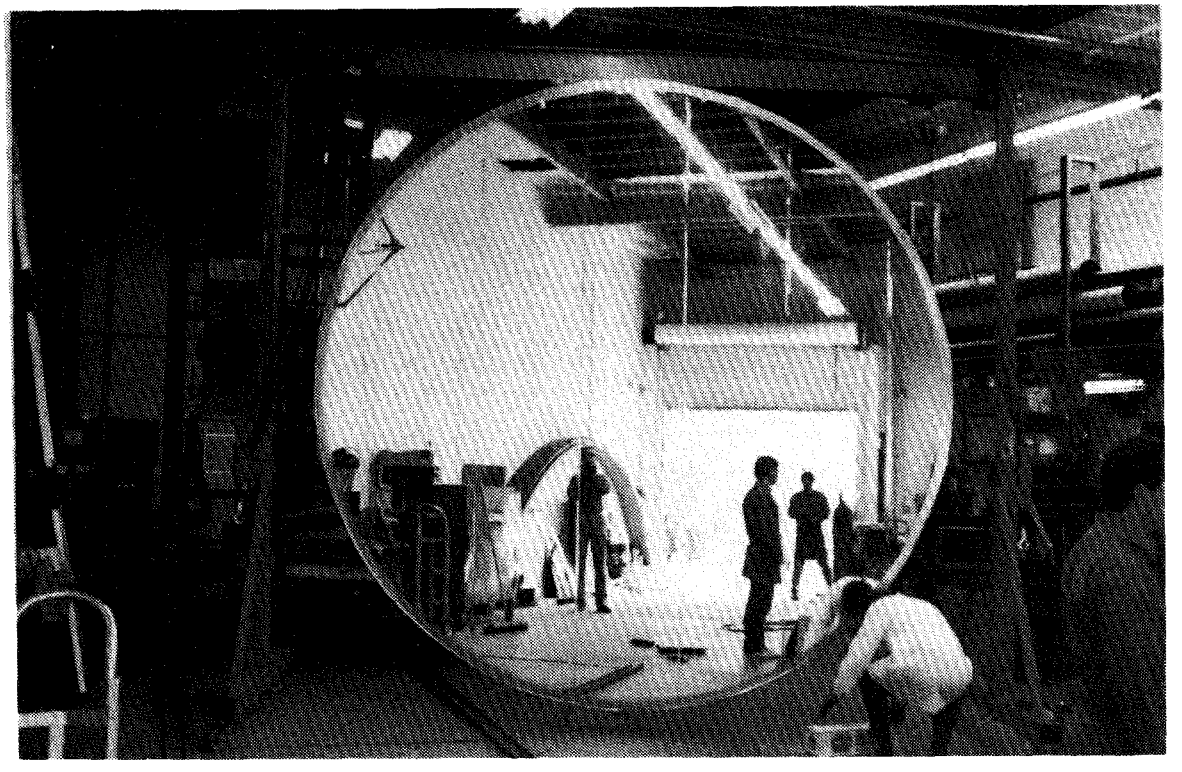

Figure 5.0-10. Facet for Faceted Stretched-Membrane Dish

6.0 FACET PRODUCTION COST ESTIMATES

A cost analysis was performed to determine the per unit cost of mirror facets at production rates of 500, 1,000, and 10,000 facets per year. The analyses included the identification of appropriate manufacturing processes, estimation of manufacturing costs, and calculation of the selling prices of the resulting facets. The following sub-sections describe the manufacturing processes and the facet cost estimates.

6.1 Facet Manufacturing Process Definition

The five processes involved in mirror facet production are as follows:

1. ring production,
2. membrane production,
3. facet assembly,
4. facet focus control system fabrication, and
5. vacuum system assembly.

The ring production process results in facet rings that are ready for membrane attachment. The membrane production process yields the facet membranes, including the reflective surfacing of the front membrane. In the facet assembly process, the membranes are tensioned and welded to the ring to produce completed mirror facets. The facet focus control system fabrication process yields the focus control valves and the valve support components that are mounted on the facet. Finally, the vacuum system assembly process involves the assembly of the blower and vacuum manifolds for the dish itself. At the end of the facet production phase, completed facets and facet focus control systems are ready to be shipped to the site and assembled onto the facet support structure.

In defining the manufacturing process, we broke the five processes into smaller individual steps for three production levels. The most appropriate fabrication processes were selected for each step. Finally, capital equipment, labor, and space requirements for each step were estimated. In the following three sub-sections, the final process selections are described for each of the three facet production rates.

6.1-1 Process Description for the 500 Facet per Year Production Rate

The 500 facet per year production rate is equivalent to the production of two facets each working day. At this rate of production, it is not worthwhile to purchase dedicated, specialized capital equipment in order to mechanize processes. Therefore, many processes are expected to be performed manually. One exception to this is that some mechanization of component fabrication is possible by performing fabrication in batches. So, for instance, a single CNC machine can be used for the automatic production of various small parts in batches, but not dedicated to production of a particular part. Another characteristic of this production rate is that many components such as the facet rings would be obtained from outside sources rather than being produced in-house.

The following paragraphs describe in detail the process steps anticipated for this production rate.

STEP 1. Ring Production

In this process step, I-beam rings are made ready for the attachment of membranes.

STEP 1.1 Receive I-Beam Rings - The I-beam rings for the facets at this production rate will be obtained from an outside vendor and will be received in lots already bent into welded. Rings will be stored on-site until needed. A forklift and overhead crane will be used to move the rings around.

STEP 1.2 Inspect I-Beams - Since the I-beams for the rings will be rolled by an outside firm, it will be necessary to inspect them upon arrival to ensure they are rolled to the correct diameter and that they are in compliance with specs. This will be done before any other processing steps.

STEP 1.3 Cut Hole for Focus Control - A hole will be cut into the rings and holes will be drilled and threaded for attachment of the focus control system.

STEP 1.4 Prepare for Membrane Welding - The I-beams will be sand-blasted and the top and bottom surfaces will be ground with a semi-automatic grinder or flycutter. The grinder will be fixed and will have a fixture to support and rotate the ring.

STEP 1.5 Fabricate Brackets - The brackets for attaching the facet to the structure will be fabricated from steel plate. A numerically-controlled machining station will be used to produce the pieces in a batch manner, with manual fixturing.

STEP 1.6 Attach Brackets - The brackets will be welded in position on the ring, using manual fixtures to provide alignment.

STEP 1.7 Paint Ring - The ring will be moved to a paint booth and painted using a standard spray gun. Rings will be set aside to cure for 24 hours before further processing.

STEP 2. Membrane Production

The front and rear membranes will be produced in a production area similar to the existing welding hall at SAIC, except that welding will be done directly on the vacuum tables.

STEP 2.1 Receive Stainless Steel - Stainless steel will be received in 24-in wide rolls and stored on-site until needed.

STEP 2.2 Inspect - The raw material will be inspected to ensure it meets specifications and is flat, straight, clean, and smooth.

STEP 2.3 Laminate Reflective Film (front membrane only) - As the stainless steel is unrolled and cut for welding, it will be laid out on a vacuum table. Reflective film will be laminated to the material using a manual laminating tool.

STEP 2.4 Weld Panels - As panels are unrolled from the coils, they will be positioned and held down on a vacuum table. A carriage-mounted roll-resistance weld head will then move along the table to weld the material together. As the welder advances, a spool behind the weld head will laminate the weld seams with reflective tape to seal the edges of the reflective film. The membranes will be rolled on tubes for transport and storage after welding.

STEP 3 Facet Assembly

The completed rings and membranes will be moved to an assembly area containing reaction rings, a manual tensioning system, and a roll-resistance welder for making the ring-to-membrane welds. There, they will be assembled together into complete mirror facets, ready for shipment.

STEP 3.1 Lay Out Rear Membrane - The rear membrane will be unrolled and held in position using mechanical clip-on tabs.

STEP 3.2 Set Up Ring in Reaction Ring - The ring will be moved to the assembly area and leveled within the reaction ring.

STEP 3.3 Lay Out Front Membrane - The front membrane will be unrolled and held in position using mechanical clip-on tabs.

STEP 3.4 Tension Membranes - A bladder-type tensioning system will be activated, to bring the membranes to the desired level of pretension.

STEP 3.5 Weld Membranes - A roll-resistance welder will be used to weld the membranes to the ring. The welder will be manually operated and have a guide to position it relative

to the facet ring. The top and bottom seams will be welded independently. Two weld passes will be made, one under reduced tension.

STEP 3.6 Remove Facet From Reaction Ring - The excess membrane material will be trimmed from the completed facet, and the facet will be removed from the reaction ring.

STEP 4 Facet Focus Control System Fabrication

The focus control valve support assembly will be machined from steel stock and assembled in the production facility. Assembled and tested facet focus control systems will be produced which are ready for shipment to the project site.

STEP 4.1 Machine Support Pieces - The mounting yoke and adjusting arm for the focus control valve will be machined from steel bar stock. The holes for bushings will be reamed to size. The mounting plate will be machined from steel plate.

STEP 4.2 Cut Pipe - The 3/4" steel pipe for the valve will be cut and threaded.

STEP 4.3 Weld - The pipe will be welded to the adjusting arm using a jig for positioning. A steel pipe nipple will be welded into the mounting plate as a feedthrough.

STEP 4.4 Machine Valve Parts - The parts for the focus control valve will be machined from Delrin and Teflon.

STEP 4.5 Assemble - All the pieces of the facet focus control system will be assembled.

STEP 4.6 Focus Control Valve Test - The completed facet focus control system will be fitted in a jig and tested for correct operation. The system will be pre-adjusted to a safe position.

STEP 5 Vacuum System Assembly

In this process step, the blower will be assembled into a protective enclosure and required wiring and piping will be completed.

STEP 5.1 Assemble Vacuum System - The blower will be mounted in an enclosure for protection from the weather.

STEP 5.2 Blower Wiring - The blower control cable will be wired.

STEP 5.3 Blower Test - The blower will be tested and the vacuum level will be set to the proper level.

6.1.2 Process Description for 1,000 Facet per Year Production Rate

Production of 1,000 facets per year yields a daily rate of four facets. As in the case of the 500 facet per year production rate, many production steps will remain manual, however the increased volume of production justifies more dedicated tooling. Differences between this production rate and the 500-

facet per year rate are that rings will be produced in-house from I-beam stock, and that components of the focus control valve will be obtained from external sources as injection-molded parts, eliminating the manual machining of those parts. Also, the blower wiring will be provided with the blower. Other changes to produce the additional quantities are additional manpower and space for additional work stations, as described below.

STEP 1. Ring Production

In this process step, I-beams are received, rolled and welded into rings, and made ready for the attachment of membranes.

STEP 1.1 Receive I-Beams - The I-beams for the facet rings will be obtained from a smelter and stored on-site until needed.

STEP 1.2 Roll Rings - The I-beams will be rolled into rings using a hydraulic ring-bending rig.

STEP 1.3 Weld Rings - The I-beam rings will be mounted in a manual jig and welded manually using a MIG welder.

STEP 1.4 Inspect Ring - The I-beams will be inspected to ensure compliance with specs. This will be done before any other processing steps.

STEP 1.5 Cut Hole for Focus Control - A hole will be cut into the rings and holes will be drilled and threaded for attachment of the focus control system.

STEP 1.6 Prepare for Membrane Welding - The I-beams will be sand-blasted and the top and bottom surfaces will be ground with a semi-automatic grinder (manual setup and feed, but with guides for positioning).

STEP 1.7 Fabricate Brackets - The brackets for attaching the facet to the structure will be fabricated from steel plate, using a numerically-controlled mill.

STEP 1.8 Attach Brackets - The brackets will be welded in position on the ring, using manual fixtures to provide alignment.

STEP 1.9 Paint Ring - The rings will be moved to a paint booth and painted using an electrostatic spray gun. Rings will be set aside to cure before further processing.

STEP 2 Membrane Production

The front and rear membranes will be produced in a production area similar to the existing weld hall at SAIC, except that welding will be done directly on the vacuum tables, eliminating the moving carriage and the tack weld step.

STEP 2.1 Receive Stainless Steel - Stainless steel will be received in 24" wide rolls and stored on-site until needed.

STEP 2.2 Inspect - The raw material will be inspected to ensure it meets specifications and is flat, straight, clean, and smooth.

STEP 2.3 Laminate Reflective Film (front membrane only) - As the stainless steel is laid out on the vacuum tables, reflective film will be laminated to the material using a manual laminator.

STEP 2.4 Weld Panels - The panels will be positioned and held down on a vacuum table. A carriage-mounted roll-resistance weld head will then move along the table to weld the material together. As the welder advances, a spool behind the weld head will laminate the weld seams with reflective tape to seal the edges of the reflective film. The membranes will be rolled on tubes for movement and storage after welding.

STEP 3 Facet Assembly

The completed rings and membranes will be moved to an assembly area containing reaction rings, a manual tensioning system, and a roll-resistance welder for making the ring-to-membrane welds. There, they will be assembled together into complete mirror facets, ready for shipment.

STEP 3.1 Lay Out Rear Membrane - The rear membrane will be unrolled and held in position using mechanical clip-on tabs.

STEP 3.2 Set Up Ring in Reaction Ring - The ring will be moved to the assembly area and leveled within the reaction ring.

STEP 3.3 Lay Out Front Membrane - The front membrane will be unrolled and held in position using mechanical clip-on tabs.

STEP 3.4 Tension Membrane - A bladder-type tensioning system will be activated, to bring the membranes to the desired level of pretension.

STEP 3.5 Weld Membranes - Using a roll-resistance welder, the membranes will be attached to the ring. The welder will be manually operated and have a guide to position it relative to the facet ring.

STEP 3.6 Remove Facet From Reaction Ring - The excess membrane material will be trimmed from the completed facet, and the facet will be removed from the reaction ring.

STEP 4 Facet Focus Control System Fabrication

The focus control valve will be obtained as an injection-molded part from an outside vendor. The support assembly will be machined from steel stock and assembled in the production facility.

Assembled and tested facet focus control systems will be produced which are ready for shipment to the project site.

STEP 4.1 Machine Support Pieces - The mounting yoke and adjusting arm will be machined from steel bar stock using a numerically-controlled mill. The holes for bushings will be reamed to size. The mounting plate will be machined from steel plate.

STEP 4.2 Cut Pipe - The pipe for the valve will be cut and threaded from 3/4" Schedule 40 steel pipe.

STEP 4.3 Weld - The pipe will be welded to the adjusting arm using a jig for positioning. A steel pipe nipple will be welded into the mounting plate to serve as a feedthrough.

STEP 4.4 Receive/Inspect Valve Parts - The parts for the focus control valve will be received and inspected for compliance with specs.

STEP 4.5 Assemble - All the pieces of the facet focus control system will be assembled.

STEP 4.6 Focus Control Valve Test - The completed facet focus control system will be fitted in a jig and tested for correct operation. The system will be pre-adjusted to a safe position.

STEP 5 Vacuum System Assembly

In this process step, the focus control system blower will be assembled into a protective enclosure and required wiring and manifolding will be completed.

STEP 5.1 Assemble Vacuum system - The blower will be mounted in an enclosure for protection from the weather. Blower electrical wiring will be provided by the blower vendor.

STEP 5.2 Blower Test - The blower will be tested and the vacuum level will be set to the proper level.

6.1.3 Process Description for 10,000 Facet per Year Production Rate

As in the scenario described in the preceding sub-section, the following process steps result in the production of complete mirror facets and facet focus control assemblies which are ready for transport to the project site. At this production rate, equivalent to 40 facets per day, significant changes to procedures are initiated. Many dedicated machines are used to automate production. The rings will be rolled in-house. Sandblasting will be replaced with an automatic wire brush/grinder which will process the I-beam material as it is received. The membranes will be produced at stations by cutting circular membranes from a single sheet of stainless steel foil that has been seamed together from several pieces. The reflective film will still be a silvered polymer laminated to the stainless steel foil, but an improved laminator will speed the process. Hydraulic grippers will replace the mechanical clips

for tensioning the membranes prior to welding, as shown in **Figures 6.1-1** and **6.1-2**. The ring-to-membrane welder will be automatic. Finally, many of the machined pieces will be cast from steel or injection molded from plastic in-house rather than being machined from bar stock or supplied from outside vendors.

The following paragraphs describe in detail the process steps involved at this production level.

STEP 1. Ring Production

In this process step, the I-beams are formed into rings, and made ready for the attachment of membranes.

STEP 1.1 Receive I-Beam - I-beams for the facets at this production rate will be obtained directly from the steel mill.

STEP 1.2 Prepare I-Beam - The I-beams will be passed through an automatic wire-brush and grinder unit. The wire brushes will clean the sides of the beam and the grinder will prepare the top and bottom surfaces for membrane attachment.

STEP 1.3 Cut Hole for Focus Control - A hole will be NC machined into the rings and holes will be threaded for attachment of the focus control system.

STEP 1.4 Roll Ring - The I-beams will be rolled into rings using in-house rolling equipment designed to produce highly flat rings.

STEP 1.5 Weld Ring - The I-beam rings will be welded, using a manual MIG welder and a permanent jig. Only a single joint will be needed.

STEP 1.6 Inspect Ring - The rings will be inspected and adjusted as necessary to obtain the needed planarity before proceeding to the membrane attachment step.

STEP 1.7 Fabricate Brackets - The brackets for attaching the facet to the structure will be cast from steel.

STEP 1.8 Install Brackets - The brackets will be welded in position on the ring, using permanent fixtures to ensure alignment.

STEP 1.9 Paint Ring - The rings will be moved to a paint booth and painted using a dry electrostatic spray gun. The paint will be heat cured before further processing.

STEP 2 Membrane Production

The front and rear membranes will be produced from a large sheet. The sheet will be formed by multiple welders operating on coil stock.

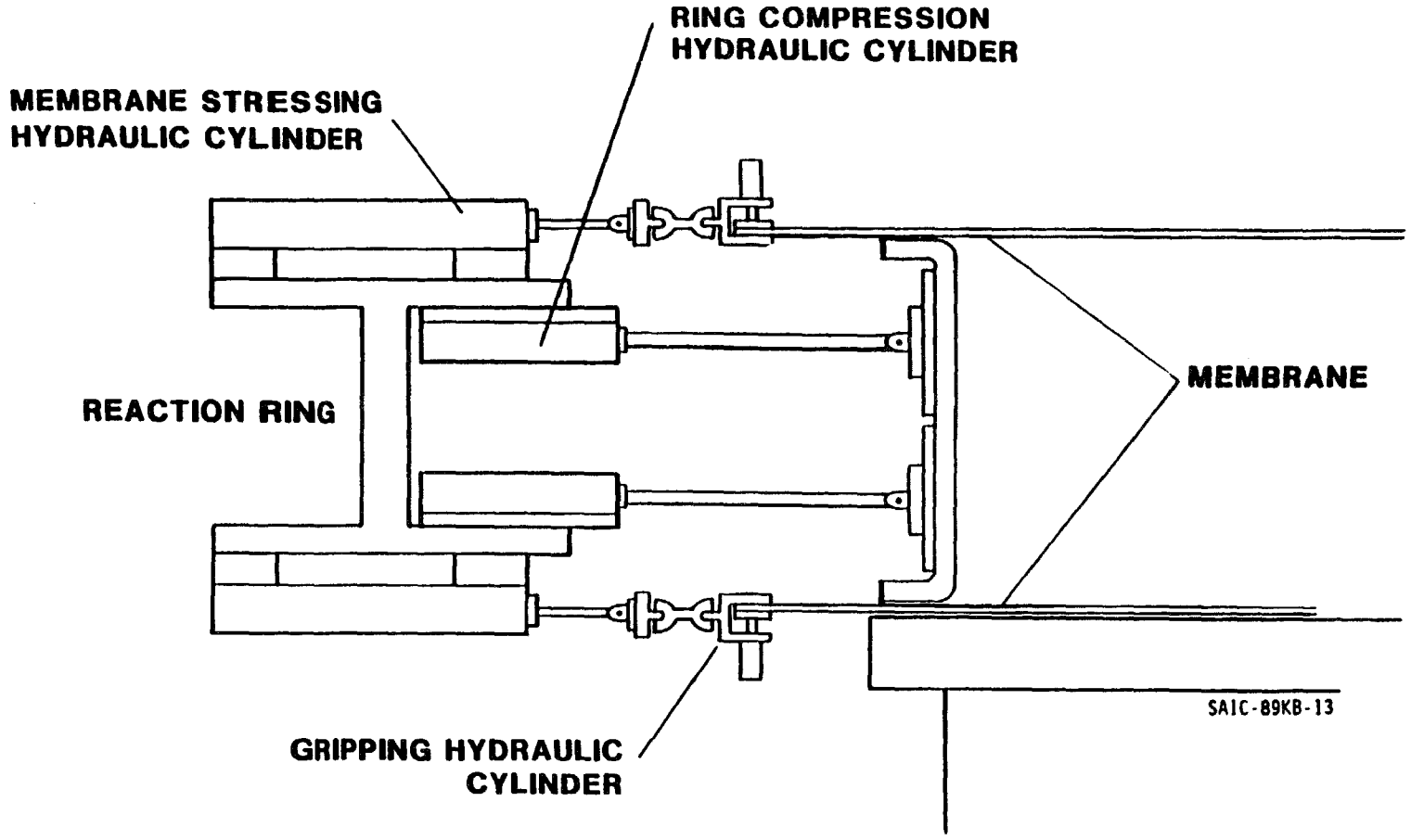

Figure 6.1-1. Commercial Membrane Tensioning System

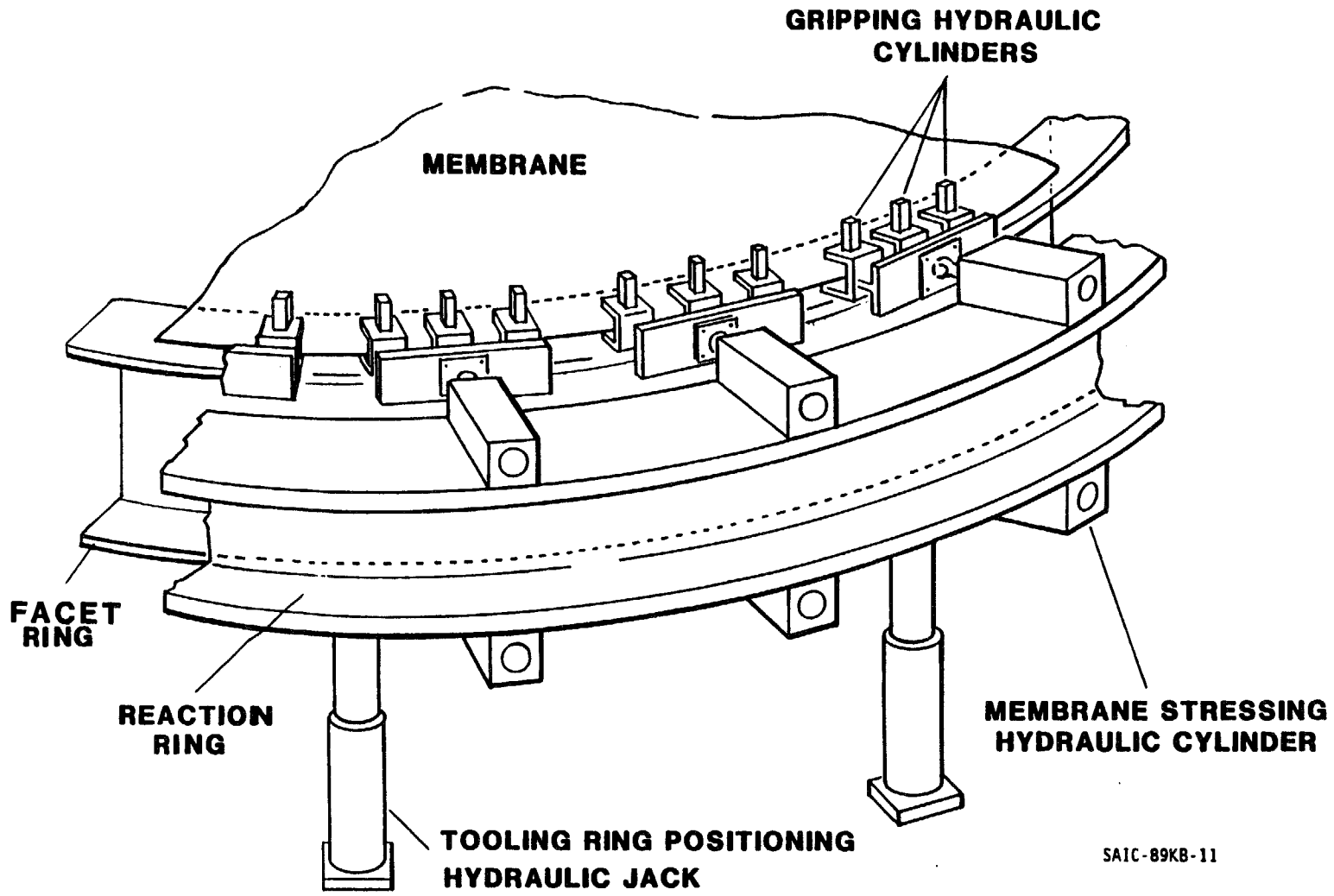

Figure 6.1-2. Commercial Tooling Concept for Ring Compression and Membrane Tensioning

STEP 2. Receive Stainless Steel - Stainless steel will be received in 36"-wide rolls and stored on-site until needed.

STEP 2.2 Inspect - The raw material will be inspected to ensure it meets specifications and is flat, straight, clean, and smooth.

STEP 2.3 Laminate Reflective Surface (front membrane only) - The reflective surface will be formed by laminating a silvered polymer reflective film onto the front membrane.

STEP 2.4 Weld Panels Into Sheets - Several panels will be welded at once as the material is unrolled from the coils. From the large sheet that is produced, round membranes will be cut and transported to the membrane attachment area using vacuum platens.

STEP 3 Facet Assembly

The completed rings and membranes will be moved to an assembly area containing reaction rings, a hydraulic tensioning system, and an automatic roll-resistance welder for making the ring-to-membrane welds. There, they will be assembled together into complete mirror facets, ready for shipment.

STEP 3.1 Lay Out Rear Membrane - The rear membrane will be placed in the tensioning fixture and held in position using hydraulic grippers.

STEP 3.2 Place Ring in Reaction Ring - The ring will be moved to the assembly area and leveled within the reaction ring.

STEP 3.3 Lay Out Front Membrane - The front membrane will be placed on the tensioning fixture and held in position using hydraulic grippers.

STEP 3.4 Tension Membrane - A hydraulic tensioning system will be activated to bring the membranes to the desired level of pretension.

STEP 3.5 Weld Membranes - The membranes will be attached to the ring using a roll-resistance welder. The welder will operate automatically, running on tracks above and below the facet to weld the top and bottom membranes to the ring at the same time.

STEP 3.6 Remove Facet From Reaction Ring - The excess membrane material will be trimmed from the completed facet, and the facet will be removed from the reaction ring.

STEP 4 Facet Focus Control System Fabrication

The focus control valve will be injection molded from plastic. The focus valve support assembly components will be cast from steel and finish machined on an automatic CNC machine, which will be shared by different jobs on a batch basis. The components will then be assembled in the production facility. Assembled and tested facet focus control systems will be produced which are ready for shipment to the project site.

STEP 4.1 Cast Support Pieces - The mounting yoke, and adjusting arm will be cast from steel. The mounting yoke, mounting plate, and hose connections will be integrated into one casting.

STEP 4.2 Machine Support Pieces - The holes for bushings will be reamed to size at a CNC machining station.

STEP 4.3 Cut Pipe - The pipe for the valve will be cut and threaded by an automatic machine.

STEP 4.4 Weld - The pipe will be welded to the adjusting arm using a jig for positioning.

STEP 4.5 Mold Valve Parts - The focus control valve components will be injection molded in-house from plastic and finish machined using a CNC machining station (shared with other processes on a batch basis).

STEP 4.6 Assemble - All the pieces of the facet focus control system will be assembled.

STEP 4.7 Focus Control Valve Test - The completed facet focus control system will be fitted in a jig and tested for correct operation. The system will be pre-adjusted to a safe position.

STEP 5 Vacuum System Assembly

In this process step, the blower will be assembled into a protective enclosure and required wiring and piping will be completed.

STEP 5.1 Assemble Vacuum System - The blower will be mounted in an enclosure for protection from the weather. Flexible tubing will be cut to lengths and fittings will be attached to form the manifold. Blower electrical wiring will be provided by the blower vendor.

STEP 5.2 Blower Test - The blower will be tested and the vacuum level will be set to the proper level.

6.2 Facet Cost Estimates

Estimates of the selling price of mirror facets were generated in a similar manner for each of the three production rates. For each step in the production process, material, labor, capital equipment, and manufacturing space requirements were estimated. Then, indirect costs for capital equipment, manufacturing space, and supervision were added to obtain the total production cost. Finally, profit was applied, and taxes and depreciation were considered to calculate the final selling price and net profit for each facet.

The two lower production rates have many production processes in common, but for the high production rate many items are mechanized. This mechanization results in reducing the cost of the facet significantly.

A summary of the basic assumptions inherent in the cost analysis follows:

50 work weeks per year

5 work days/week, 1 shift

Labor Costs:

Laborers:	$9/hr		
Clerical:	$15/hr		
Line Supervisors:	$20/hr		
Engineers:	$30/hr		
Managers:	$40/hr		
Laborer Overhead Rates:	500/yr	1,000/yr	10,000/yr
	70%	70%	50%

Useful Life of Plant Equipment:	10 yrs
Depreciation for Tax Purposes:	7-year straight-line
Cost of Production Space:	$0.67/month/ft^2
Cost of Office Space:	$1/month/ft^2
Gross Profit:	15% of Total Production Cost
Taxes on Net Profit:	38% (combined State and Federal)

The results of the cost analyses are summarized in **Table 6.2-1**. In the table are the costs of the reflective film, a major cost component, other direct materials costs, indirect costs, and the selling price of the facets (FOB factory). Also included in the table are the number of labor man-hours per facet and the total capital cost for the manufacturing facility needed for each production rate. As shown in the table, we can see the estimated selling price of facets drops from $\$113/m^2$ to just over $\$50/m^2$ as the production rate is increased from 500 to 10,000 facets per year. The reflective film cost was held constant, so the price reductions are due to reductions in other direct and indirect costs. These reductions are the result of in-house production of components, increased mechanization to minimize man-hour requirements, and reduced overhead due to economies of scale. The advantage

of going to large-scale production is clear. The capital equipment requirement for the large-scale facility is significantly higher than that for the lower production rates, but it becomes a minor cost component on a per-facet basis because it is amortized over the large number of facets produced.

Table 6.2-1. Summary of Costs for Facet Production

Annual Production Rate	500	1,000	10,000
Reflective Film	$198	$198	$198
Other Direct Costs	$548	$476	$197
Indirect Costs	$399	$272	$122
Selling Price (FOB Factory)	$1,145 $112.5/m^2	$946 $93.0/m^2	$517 $51/m^2
Labor Required (man-hrs)	18.7	20.7	4.55
Capital Equipment	$208K	$387K	$1,720K

Tables 6.2-2, **6.2-3**, and **6.2-4** give the detailed cost estimates for each of the three production rates. In these estimates, capital equipment costs include costs for development required for special tooling and equipment. Other capital equipment costs are very conservative estimates. Labor hours and production space estimates were based on an evaluation of the activities involved in each of the process step and on how much working and storage space would be required.

Table 6.2-2 gives the cost estimate for a production rate of 500 facets per year. In this case, the total labor force needed for production comes to about four full-time employees. One full-time supervisor/plant manager and half-time of an engineer and clerical person were felt to be sufficient for supervision and support to the manufacturing facility.

In **Table 6.2-3**, the work force for production of 1,000 facets per year is shown to be increased to about ten full-time employees. This is more than double the number needed for production of 500 facets because more component fabrication is done in-house at this production level. The number of indirect personnel remained the same as the 500 facet per year production level, reducing the overhead of the operation.

Table 6.2-4 gives the cost analysis for the 10,000 facet per year production rate. The most significant changes are the large increase in production space and capital equipment to allow production of more components in-house, and the reduction in per-facet labor costs due to increased mechanization of

Table 6.2-2. Cost Estimate for Facet Production at 500 Facets per Year

500 /yr Production Rate
2 /day

$15.3 Hourly Labor Rate
$80 Production Space/m^2/yr
$120 Office Space/m^2/yr

Process Step	Labor Hours	Materials Qty.	Units	Cost	Type	Space (m^2)	Capital Eqpt. Cost ($K)	Description	Labor Cost	Mat'ls Cost	Total Cost
1.0 Ring Production											
1.1 Receive I-Beam Rings	0.10	1	ea	$150.00	M8 x 6.5 I Beam Ring	20	20	Fork Lift	2	150	152
							10	Overhead Crane	0	0	0
1.2 Inspect Ring	0.10					20	5	Laser Leveler	2	0	2
1.3 Cut Hole for Focus Control	0.75						2	Cutting Torch	11	0	11
							2	Mag-Base Drill	0	0	0
1.4 Prepare for Membrane Welding	4.00						20	Grinder/Flycutter	61	0	61
1.5 Fabricate Brackets	1.00	20	lb	$0.44	Steel Plate	10	50	NC Mill	15	9	24
		10	ea	$1.00	Weld Rod				0	10	10
1.6 Attach Brackets	0.50	5	ea	$1.00	Weld Rod		5	MIG Welder	8	5	13
1.7 Paint Ring	0.50	1	gal	$10.00	Paint	30	5	Spray Painter	8	10	18
2.0 Membrane Production									0	0	0
2.1 Receive Stainless Steel	0.10	19.2	m^2	$2.20	3 mil 201 SS foil	5			2	42	44
2.2 Inspect	0.05								1	0	1
2.3 Laminate Reflective Film	2.00	9.2	m^2	$21.53	ECP-305 Reflective Film		5	Laminator	31	198	229
2.4 Weld Panels	4.00					15	15	Roll-Resistance Welder	61	0	61
							20	Carriage for Welder	0	0	0
3.0 Facet Assembly									0	0	0
3.1 Lay Out Rear Membrane	0.50					20	10	Gantry Crane	8	0	8
							5	Clip-On Tabs	0	0	0
3.2 Set Up Ring in Tooling Ring	0.50						5	Reaction Ring	8	0	8
3.3 Lay Out Front Membrane	0.50								8	0	8
3.4 Tension Membrane	0.10						2	Bladder System	2	0	2
							2	Compressor	0	0	0
3.5 Weld Membranes	1.00						5	Welder	15	0	15
							10	Carriage/Guide	0	0	0
3.6 Remove From Reaction Ring	0.50								8	0	8
4.0 Facet Focus Control System Fabrication									0	0	0
4.1 Machine Support Pieces	1.00	2	lb	$0.44	Steel stock	20			15	1	16
4.2 Cut Pipe	0.10	4	ft	$0.55	Steel Pipe				2	2	4
4.3 Weld	0.10								2	0	2
4.4 Machine Valve Parts	0.30	1	lb	$10.00	Delrin				5	10	15
4.5 Assemble	0.10	1	lot	$1.00	Screws, Misc				2	1	3
4.6 Focus Control Valve Test	0.10					10	10	Test Jig	2	0	2
5.0 Vacuum System Assembly									0	0	0
5.1 Assemble Vacuum System	0.50	1	ea	$18.75	Per-Facet Blower Cost	10			8	19	26
		1	ea	$1.67	Enclosure				0	2	2
5.2 Blower Wiring	0.20	1	lot	$1.67	Wire, Tubing				3	2	5
5.3 Blower Test	0.10								2	0	2
Total Direct Costs	18.70	Man-hrs				160	$208.0	K	$286	$460	$746

Indirect Costs	Qty.	Units	Cost		
Capital Eqpt. (10 yr lifetime)					42
Manufacturing Space	160	m^2	$0.16		26
Office Space	50	m^2	$0.24		12
Line Supervisor	4	hrs	$20.00	80	80
Engineering	2	hrs	$30.00	60	60
Clerical	2	hrs	$15.00	30	30
Total Production Costs				$456	$460	$995

Gross Profit (15%)			$149
Depreciation (7-year straight-line)	($59)		
Net Taxable Income	$90		
Taxes (38% of Taxable Income)	$34		
Net Profit	$115	10.1% of sales	
Selling Price			$1,145
			$112.5 /m^2

Table 6.2-3. Cost Estimate for Facet Production at 1,000 Facets per Year

$15.30 Hourly Labor Rate
$80 Production Space/m^2/yr
$120 Office Space/m^2/yr

1000 /yr Production Rate
4 /day

Process Step	Labor Hours	Materials Qty.	Units	Cost	Type	Space (m^2)	Capital Eqpt. Cost ($K)	Description	Labor Cost	Mat'ls Cost	Total Cost
1.0 Ring Production											
1.1 Receive I-Beams	0.10	260	lb	$0.24	M8 x 6.5 I Beam Ring	30	20	Fork Lift	2	62	64
							10	Overhead Crane	0	0	0
1.2 Roll Rings	2.00					10	100	Ring Roller	31	0	31
1.3 Weld Ring	0.25						5	MIG Welder	4	0	4
1.4 Inspect Ring	0.10					20	5	Laser Leveler	2	0	2
1.5 Cut Hole for Focus Control	0.75						2	Cutting Torch	11	0	11
							2	Mag-Base Drill	0	0	0
1.6 Prepare for Membrane Welding	4.00						20	Grinder/Flycutter	61	0	61
1.7 Fabricate Brackets	1.00	20	lb	$0.35	Steel Plate	10	50	NC Mill	15	7	22
		10	ea	$1.00	Weld Rod				0	10	10
1.8 Attach Brackets	0.50	5	ea	$1.00	Weld Rod		5	MIG Welder	8	5	13
1.9 Paint Ring	0.50	1	gal	$10.00	Paint	40	10	Electrostatic Paint Sys.	8	10	18
2.0 Membrane Production									0	0	0
2.1 Receive Stainless Steel	0.10	19.2	m^2	$1.98	3 mil 201 SS foil	10			2	38	40
2.2 Inspect	0.05								1	0	1
2.3 Laminate Reflective Film	2.00	9.2	m^2	$21.53	ECP-305 Reflective Film		10	Laminator (2)	31	198	229
2.4 Weld Panels	4.00					30	30	2 Roll-Resistance Welders	61	0	61
							40	Carriage for Welder (2)	0	0	0
3.0 Facet Assembly									0	0	0
3.1 Lay Out Rear Membrane	0.50					40	10	Gantry Crane	8	0	8
							10	Clip-On Tabs (2 sets)	0	0	0
3.2 Set Up Ring in Tooling Ring	0.50						10	Reaction Ring (2)	8	0	8
3.3 Lay Out Front Membrane	0.50								8	0	8
3.4 Tension Membrane	0.10						4	Bladder System (2)	2	0	2
							4	Compressor	0	0	0
3.5 Weld Membranes	1.00						10	Welder (2)	15	0	15
							20	Carriage/Guide (2)	0	0	0
3.6 Remove From Reaction Ring	0.50								8	0	8
4.0 Facet Focus Control System Fabrication									0	0	0
4.1 Machine Support Pieces	1.00	2	lb	$0.35	Steel stock	25			15	1	16
4.2 Cut Pipe	0.10	4	ft	$0.50	3/4" Sch 40 Steel Pipe				2	2	4
4.3 Weld	0.25								4	0	4
4.4 Receive/Inspect Valve Parts	0.10	1	lot	$5.00	Injection-Molded Parts				2	5	7
4.5 Assemble	0.10	1	lot	$1.00	Screws, Misc				2	1	3
4.6 Focus Control Valve Test	0.10					10	10	Test Jig	2	0	2
5.0 Vacuum System Assembly									0	0	0
5.1 Assemble Vacuum System	0.50	1	ea	$16.88	Per-Facet Blower Cost	10			8	17	25
		1	ea	$1.67	Enclosure				0	2	2
5.2 Blower Test	0.10								2	0	2
Total Direct Costs	20.70	Man-hrs				235	$387 K		$317	$358	$674

Indirect Costs	Qty.	Units	Cost		
Capital Eqpt. (10 yr lifetime)					39
Manufacturing Space	235	m^2	$0.08		19
Office Space	50	m^2	$0.12		6
Line Supervisor	2	hrs	$20.00	40	40
Engineering	1	hrs	$30.00	30	30
Clerical	1	hrs	$15.00	15	15
Total Production Costs				$402	$358	$823
Gross Profit (15%)						$123
Depreciation (7-year straight-line)			($55)			
Net Taxable Income			$68			
Taxes (38% of Taxable Income)			$26			
Net Profit			$98	10.3% of sales		
Selling Price						$946
						$93.0 /m^2

Table 6.2-4. Cost Estimate for Facet Production at 10,000 Facets per Year

10000 /yr Production Rate
40 /day

$13.50 Hourly Labor Rate
$80 Production Space/m^2/yr
$120 Office Space/m^2/yr

Process Step	Labor Hours	Materials Qty.	Units	Cost	Type	Space (m^2)	Capital Eqpt. Cost ($K)	Description	Labor Cost	Mat'ls Cost	Total Cost
1.0 Ring Production											
1.1 Receive I-Beam	0.05	260	lb	$0.21	M8 x 6.5 I Beam	60	25	Fork Lift	1	55	55
							20	Overhead Crane	0	0	0
1.2 Prepare Ring	0.20					60	50	Grinder/Wire Brush	3	0	3
1.3 Cut Hole for Focus Control	0.20						10	Hole Cutter	3	0	3
1.4 Roll Rings	0.20					25	300	3 Ring Rollers	3	0	3
1.5 Weld Ring	0.25						20	Welder	3	0	3
1.6 Inspect Ring	0.10					25	10	Laser Leveler	1	0	1
1.7 Fabricate Brackets	0.10	20	lb	$0.33	Steel	10	75	Casting Furnace	1	7	8
						10	50	NC Mill	0	0	0
1.8 Attach Brackets	0.20	1	lot	$5.00	Welding Rod	50	20	MIG Welders	3	5	8
1.9 Paint Ring	0.25	1	gal	$10.00	Paint	50	20	2 Electrostatic Paint Sys.	3	10	13
2.0 Membrane Production									0	0	0
2.1 Receive Stainless Steel	0.10	19.2	m^2	$1.98	3 mil 201 SS foil	25			1	38	39
2.2 Inspect	0.05								1	0	1
2.3 Laminate Reflective Surface	0.20	9.2	m^2	$21.53	ECP-305		10	Laminator	3	198	201
2.4 Weld Panels into Sheets	0.50					50	200	3 Multiple Weld Stations	7	0	7
							100	Cutters for Membranes	0	0	0
3.0 Facet Assembly									0	0	0
3.1 Lay Out Rear Membrane	0.20					125	100	5 Gantry Cranes	3	0	3
							150	5 Hydraulic Tensioning Sys	0	0	0
3.2 Place Ring in Reaction Ring	0.10						50	5 Reaction Rings	1	0	1
3.3 Lay Out Front Membrane	0.20								3	0	3
3.4 Tension Membrane	0.10								1	0	1
3.5 Weld Membranes	0.50						125	5 Automatic Welders	7	0	7
							100	5 Carriages/Guides	0	0	0
3.6 Remove From Reaction Ring	0.10								1	0	1
4.0 Facet Focus Control System Fabrication									0	0	0
4.1 Cast Support Pieces	0.05	2	lb	$0.35	Steel	25	75	Casting Furnace	1	1	1
4.2 Machine Support Pieces	0.05					10	50	NC Mill	1	0	1
4.3 Cut Pipe	0.05	4	ft	$0.40	3/4" Sch 40 Steel Pipe	10	50	Automatic Screw Machine	1	2	2
4.4 Weld	0.20								3	0	3
4.5 Mold Valve Parts	0.05	1	lot	$2.00	Plastic	30	100	Injection Molder	1	2	3
						10			0	0	0
4.6 Assemble	0.10	1	lot	$1.00	Screws, Misc	20			1	1	2
4.7 Focus Control Valve Test	0.10					20	10	Automated Test Jig	1	0	1
5.0 Vacuum System Assembly									0	0	0
5.1 Assemble Vacuum System	0.25	1	ea	$15.00	Per-Facet Blower Cost	50			3	15	18
		1	ea	$1.33	Enclosure				0	1	1
5.2 Blower Test	0.10								1	0	1
Total Direct Costs	4.55	Man-hrs				665	$1,720	K	$61	$334	$395

Indirect Costs	Qty.	Units	Cost	
Capital Eqpt. (10 yr lifetime)				17
Manufacturing Space	665	m^2	$0.01	5
Office Space	200	m^2	$0.01	2
Line Supervisors	0.6	hrs	$20.00	12
Managers	0.2	hrs	$40.00	8
Engineering	0.2	hrs	$30.00	6
Clerical	0.2	hrs	$15.00	3
Total Production Costs				$90 $334 $449
Gross Profit (15%)				$67
Depreciation (7-year straight-line)	($25)			
Net Taxable Income	$43			
Taxes (38% of Taxable Income)	$16			
Net Profit	$51		9.9% of sales	
Selling Price				$517
				$51 /m^2

the production processes. At this level, a production force of about 23 full-time employees is estimated to be required. The support staff for this production rate is estimated to consist of a plant manager, three line supervisors, one full-time production engineer, and one secretary.

6.3 Cost Quotes and Estimates

The following material cost estimates were obtained in support of the facet production cost estimates.

1. M8X6.5 I-Beam - Estimates were obtained for the three production levels from Chaparral Steel Company in Texas. The estimates were $21 - $24/hundredweight. The $24 figure was used in the estimate for the two lower production rates, and the $21 figure for the high production case.

2. Plate Steel - Jorgensen Steel Co. gave estimates for 1/4" hot rolled steel plate as follows:

5 Ton/yr	$43.50/100#
10 Ton/yr	$34.56/100#
100 Ton/yr	$32.55/100#

   These costs were used for the facet support components, and the $32.55 cost was used for raw steel costs for casting in the high-production case.

3. Steel Pipe - Jorgensen Steel Co. gave estimates for 100 foot lengths of 3/4" Schedule 40 steel pipe as follows:

1 Ton/yr	$55.30/100 ft
2 Ton/yr	$50.30/100 ft
20 Ton/yr	$40.30/100 ft

   These estimates were used for the focus control pipe. Costs for aluminum pipe, as used in the prototype, were approximately three times as high as steel pipe, so steel pipe was substituted in production.

4. Stainless Steel Foil - Allegheny Ludlum was contacted to obtain updated costs for Type 201 half-hard stainless steel. The following price quotes were obtained:

12 Ton/yr	$ 2.20/ft^2
24 Ton/yr	$ 1.98/ft^2
240 Ton/yr	$ 1.98/ft^2

5. Reflective Film - A single estimate of $21.53/m^2 ($2/ft^2) for ECP-305 reflective film was used. Talks with 3M indicated that significant price reductions for the volumes we are considering would not be possible.

7.0 CONCLUSIONS

Phase 1 of the "Stretched-Membrane Facet Development Project" has been successful in demonstrating the technical feasibility and potential cost effectiveness of a multi-facet stretched-membrane dish for a 25 kW_e power production unit. The optical performance of the facets produced under this project meet the requirements that were outlined in the project statement of work. The viability of elastic deformation of a stretched-membrane for dish concentrator applications has been demonstrated.

In the performance of this contract, SAIC has made advances in applying stretched-membrane technology to high stress elastic deformation conditions, and has developed low cost, high reliability facet focus control system components. The production cost estimates for the facets are in line with cost goals with the Solar Thermal Program.

The success of Phase 1 of the project has prepared SAIC and other team members for continuation of the project into Phase 2 with the fabrication and testing of a complete 75 kW_{th} faceted stretched-membrane dish.

8.0 REFERENCES

1. Science Applications International Corporation, San Diego, CA, "Selection and Design of a Stretched-Membrane Heliostat for Today's Market", SAND89-7040, January 1990.

2. Science Applications International Corporation, San Diego, CA, "An Improved Design for Stretched-Membrane Heliostats", SAND89-7027, June 1989.

3. L.M. Murphy, "Moderate to Large Axisymmetric Deformation of Optical Membrane Surfaces", Solar Energy Research Institute, Golden, CO April 1986.

4. R.J. Roark and W.C. Young, "Formulas for Stress and Strain", Fifth Edition, New York, McGraw Hill, 1982.

5. J. A. Peterka and Z. Tan, "Wind Load Design guide for Ground-Based Heliostats", Colorado State University.

UNLIMITED DISTRIBUTION
INITIAL DISTRIBUTION
REVISION 4/2/91/trm

U.S. Department of Energy (5)
Forrestal Building
Code CE-314
1000 Independence Avenue, SW
Washington, DC 20585
Attn: M. Scheve
S. Gronich

U.S. Department of Energy (2)
Forrestal Building
Code CE-33
1000 Independence Avenue, SW
Washington, DC 20585
Attn: B. Annan

U.S. Department of Energy (3)
Albuquerque Operations Office
P.O. Box 5400
Albuquerque, NM 87115
Attn: C. Garcia
G. Tennyson
N. Lackey

U.S. Department of Energy
San Francisco Operations Office
1333 Broadway
Oakland, CA 94612
Attn: R. Hughey

AAI Corporation
P. O. Box 6787
Baltimore, MD 21204

Acurex Corporation (2)
555 Clyde Avenue
Mountain View, CA 94039
Attn: J. Schaefer
H. Dehne

Advanced Thermal Systems
7600 East Arapahoe
Suite 319
Englewood, CO 80112
Attn: D. Gorman

Arizona Public Service Company
P.O. Box 53999
M/S 9110
Phoenix, AZ 85072-3999
Attn: W. J. McGuirk

Arizona Solar Energy Office
3800 North Central
Phoenix, AZ 85012
Attn: R. Williamson

Australian National University
Department of Engineering Physics
P. O. Box 4
Canberra ACT 2600 AUSTRALIA
Attn: S. Kaneff

Barber-Nichols Engineering
6325 West 55th Avenue
Arvada, CO 80002
Attn: R. Barber

Battelle Pacific Northwest
Laboratory (2)
P.O. Box 999
Richland, WA 99352
Attn: T. A. Williams
D. Brown

BDM Coporation
1801 Randolph Street
Albuquerque, NM 87106
Attn: W. Schwinkendorf

Bechtel National, Inc.
50 Beale Street
50/15 D8
P. O. Box 3965
San Francisco, CA 94106
Attn: P. DeLaquil

Black & Veatch Consulting
Engineers
P.O. Box 8405
Kansas City, MO 64114
Attn: J. C. Grosskreutz

Tom Brumleve
1512 Northgate Road
Walnut Creek, CA 94598

California Energy Commission
1516 Ninth Street, M-S 43
Sacramento, CA 95814
Attn: A. Jenkins

California Polytechnic University
Dept. of Mechanical Engineering
Pomona, CA 91768
Attn: W. Stine

California Public Utilities Com.
Resource Branch, Room 5198
455 Golden Gate Avenue
San Francisco, CA 94102
Attn: T. Thompson

Cummins Engine Co.
MC 60125
P. O. Box 3005
Columbus, IN 47202-3005
Attn: R. Kubo

Dan Ka
3905 South Mariposa
Englewood, CO 80110
Attn: D. Sallis

DLR
Pfaffenwaldring 38-40
7000 Stuttgart 80 WEST GERMANY
Attn: R. Buck

DSET
P. O. Box 1850
Black Canyon Stage I
Phoenix, AZ 85029
Attn: G. Zerlaut

Electric Power Research
Institute
P.O. Box 10412
Palo Alto, CA 94303
Attn: J. Schaeffer

Engineering Perspectives
20 19th Avenue
San Francisco, CA 94121
Attn: John Doyle

Energy Technology Engr. Center
Rockwell International Corp.
P. O. Box 1449
Canoga Park, CA 91304
Attn: W. Bigelow

ENTECH, Inc.
P. O. Box 612246
DFW Airport, TX 75261
Attn: R. Walters

Florida Solar Energy Center
300 State Road 401
Cape Canaveral, FL 32920
Attn: Library

Ford Aerospace
Ford Road
Newport Beach, CA 92663
Attn: R. Babbe

Foster Wheeler Solar Development
Corporation (2)
12 Peach Tree Hill Road
Livingston, NJ 07039
Attn: M. Garber
R. Zoschak

Garrett Turbine Engine Co.
111 South 34th Street
P. O. Box 5217
Phoenix, AZ 85010
Attn: E. Strain

Georgia Power (2)
7 Solar Circle
Shenandoah, GA 30265
Attn: W. King

Harris Corporation (2)
Government and Aerospace
Systems Division
P. O. Box 9400
Melbourne, FL 32902
Attn: K. Schumacher

Industrial Solar Technologies
5775 West 52nd Avenue
Denver, CO 80212
Attn: R. Gee

Institute of Gas Technology
34245 State Street
Chicago, IL 60616
Attn: Library

ISEIR
951 Pershing Drive
Silver Spring, MD 20910
Attn: A. Frank

Jet Propulsion Laboratory
4800 Oak Grove Drive
Pasadena, CA 91109
Attn: M. Alper

LaJet Energy Company
P. O. Box 3599
Abilene, TX 79604
Attn: M. McGlaun

Lawrence Berkeley Laboratory
MS 90-2024
One Cyclotron Road
Berkeley, CA 94720
Attn: A. Hunt

Luz International (2)
924 Westwood Blvd.
Los Angeles, CA 90024
Attn: D. Kearney

3M-Energy Control Products (2)
207-1W 3M Center
St. Paul, MN 55144
Attn: R. Dahlen

Mechanical Technology, Inc. (2)
968 Albany Shaker Road
Latham, NY 12110
Attn: G. Dochat
J. Wagner

Meridian Corporation
4300 King Street
Alexandria, VA 22302
Attn: D. Kumar

NASA Lewis Research Center (4)
21000 Brook Park Road
Cleveland, OH 44135
Attn: R. Beremand 500-215
R. Evans 500-210
J. Savino 301-5
R. Corrigan 500-316

Nevada Power Co.
P. O. Box 230
Las Vegas, NV 89151
Attn: Mark Shank

Pacific Gas and Electric Company (2)
3400 Crow Canyon Road
San Ramon, CA 94526
Attn: G. Braun
J. Iannucci

Polydyne, Inc.
1900 S. Norfolk Street, Suite 209
San Mateo, CA 94403
Attn: P. Bos

Power Kinetics, Inc.
415 River Street
Troy, NY 12180-2822
Attn: W. Rogers

Renewable Energy Institute
1001 Connecticut Ave. NW
Suite 719
Washington, DC 20036
Attn: K. Porter

Rocketdyne Division
6633 Canoga Park Ave.
Canoga Park, CA 91304
Attn: W. Marlatt

San Diego Gas and Electric Company
P.O. Box 1831
San Diego, CA 92112
Attn: R. Figueroa

SCE
P. O. Box 800
Rosemead, CA 91770
Attn: P. Skvarna

Schlaich, Bergermann & Partner
Hohenzollernstr. 1
D - 7000 Stuttgart 1
West Germany
Attn: W. Schiel

Sci-Tech International
Advanced Alternative Energy
5673 W. Las Positas Blvd.,Suite 205
P.O. Box 5246
Pleasanton, CA 84566
Attn: U. Ortabasi

Science Applications International
Corporation (2)
10343 Roselle Street, Suite G
San Diego, CA 92121
Attn: K. Beninga

Solar Energy Research Institute (5)
1617 Cole Boulevard
Golden, CO 80401
Attn: B. Gupta
L. M. Murphy
G. Jorgensen
T. Wendelin
A. Lewandowski

Solar Kinetics, Inc. (2)
P.O. Box 540636
Dallas, TX 75354-0636
Attn: J. A. Hutchison
P. Schertz
D. Konnerth

Solar Power Engineering Company
P.O. Box 91
Morrison, CO 80465
Attn: H. Wroton

Solar Steam
P. O. Box 32
Fox Island, WA 98333
Attn: D. Wood

SPECO
P. O. Box 91
Morrison, CO 80465
Attn: W. Hart

SRS Technologies
990 Explorer Blvd., NW
Huntsville, AL 35806
Attn: R. Bradford

Stearns Catalytic Corporation
P.O. Box 5888
Denver, CO 80217
Attn: T. E. Olson

Stirling Thermal Motors
2841 Boardwalk
Ann Arbor, MI 48104
Attn: B. Ziph

Sun Power, Inc.
6 Byard Street
Athens, OH 45701
Attn: W. Beale

Tom Tracey
6922 South Adams Way
Littleton, CO 80122

United Solar Tech, Inc.
3434 Martin Way
Olympia, WA 98506
Attn: R. Kelley

University of Chicago
Enrico Fermi Institute
5640 Ellis Avenue
Chicago, IL 60637
Attn: J. O'Gallagher

University of Houston
Solar Energy Laboratory
4800 Calhoun
Houston, TX 77704
Attn: L. Vant-Hull

University of Utah
Mechanical and Industrial
Engineering
Salt Lake City, UT 84112
Attn: B. Boehm

Eric Weber
302 Caribbean Lane
Phoenix, AZ 85022

WG Associates
6607 Stonebrook Circle
Dallas, TX 75240
Attn: V. Goldberg

1840 R. E. Loehman
1846 D. H. Doughty
1846 C. S. Ashley
3141 S. A. Landenberger (5)
3145 Document Processing (8)
For DOE/OSTI
3151 G. C. Claycomb
6000
6200 B. W. Marshall
6210
6215 C. P. Cameron
6215 R. M. Houser
6216 C. E. Tyner
6216 L. Yellowhorse
6216 D. J. Alpert
6216 J. W. Grossman
6216 T. R. Mancini (30)
6216 J. E. Pacheco
6217 P. C. Klimas
6217 K. L. Linker
6217 R. B. Diver
6220 D. G. Schueler
6221 E. C. Boes
6223 G. J. Jones
6224 A. R. Mahoney
7470 J. L. Ledman
7476 F. P. Gerstle
7476 S. T. Reed
8523 R. C. Christman